



EOARD FA8655-04-1-3076

2nd Six Monthly Report

Electronically Reconfigurable Microwave Lens Antennas

Liang Xue, Vincent Fusco IEEE Fellow

High Frequency Research Laboratories
The Institute of Electronics, Communications and Information Technology
(ECIT)
Queens University Belfast
Northern Ireland Science Park
Queens Road
Queens Island
Belfast BT3 9DT
N Ireland

Ph: 44 (0)28 9097 1806
Fax: 44 (0)28 9097 1702
Email: v.fusco@ecit.qub.ac.uk
Web: www.ecit.qub.ac.uk

Abstract

The purpose of this report is to present the results of further investigations into the operation and design of two-dimensional Luneburg Lenses at 24 GHz, with the possibility for electronic control of their behavior. Various lens design techniques are illustrated; these include a holey dielectric lens (drilled dielectric) and, a holey plate lens (etched holes on the upper metal plate). Ray tracing theory is presented which shows the general properties of the gradient index lens. These results indicate that it may be possible to synthesize a tuneable lens whose focal length and /or radiation pattern can be adjusted by electronic modification of the lens dielectric properties. In addition a uniform outer layer lens and a two-shell lens are also demonstrated. Some preliminary investigations are presented with regard to the general properties of Liquid Crystal materials for tuneable lens use. Also we present preliminary design work on a MMIC reflection amplifier for ultimate deployment in active planar lens reflector for RCS enhancement.

Report Documentation Page

*Form Approved
OMB No. 0704-0188*

Public reporting burden for the collection of information is estimated to average 1 hour per response, including the time for reviewing instructions, searching existing data sources, gathering and maintaining the data needed, and completing and reviewing the collection of information. Send comments regarding this burden estimate or any other aspect of this collection of information, including suggestions for reducing this burden, to Washington Headquarters Services, Directorate for Information Operations and Reports, 1215 Jefferson Davis Highway, Suite 1204, Arlington VA 22202-4302. Respondents should be aware that notwithstanding any other provision of law, no person shall be subject to a penalty for failing to comply with a collection of information if it does not display a currently valid OMB control number.

1. REPORT DATE 13 DEC 2005	2. REPORT TYPE N/A	3. DATES COVERED		
4. TITLE AND SUBTITLE Electronically Reconfigurable Microwave Lens Antennas		5a. CONTRACT NUMBER		
		5b. GRANT NUMBER		
		5c. PROGRAM ELEMENT NUMBER		
6. AUTHOR(S)		5d. PROJECT NUMBER		
		5e. TASK NUMBER		
		5f. WORK UNIT NUMBER		
7. PERFORMING ORGANIZATION NAME(S) AND ADDRESS(ES) Queen's University Belfast Ashby Building Belfast BT9 5AH United Kingdom		8. PERFORMING ORGANIZATION REPORT NUMBER		
9. SPONSORING/MONITORING AGENCY NAME(S) AND ADDRESS(ES)		10. SPONSOR/MONITOR'S ACRONYM(S)		
		11. SPONSOR/MONITOR'S REPORT NUMBER(S)		
12. DISTRIBUTION/AVAILABILITY STATEMENT Approved for public release, distribution unlimited.				
13. SUPPLEMENTARY NOTES The original document contains color images.				
14. ABSTRACT				
15. SUBJECT TERMS				
16. SECURITY CLASSIFICATION OF:		17. LIMITATION OF ABSTRACT UU	18. NUMBER OF PAGES 53	19a. NAME OF RESPONSIBLE PERSON
a. REPORT unclassified	b. ABSTRACT unclassified			

List of Contents

List of Symbols, Variables and Acronyms

I. Introduction

II. Luneburg Lens Synthesis Techniques

(2.1) Holey Dielectric Lens (Fractional Volume Permittivity Control)

(2.1.1) Permittivity Distribution Control

(2.1.2) Lens Design

(2.1.3) Simulation and Measurement

(2.1.4) Lens Matching using 3-D Tapered Microstrip Lines

(2.2) Holey Plate Lens

(2.2.2) Holey Metal Plate Luneburg Lens operated in TE mode

(1) Range of Parameters required for Luneburg Lens Application

(2) Holey Plate lens based on Standard Material (Taconic CER 10)

(2.2.3) Holey Metal Plate Luneburg Lens operated in TEM mode

III. Ray Tracing Lens

(3.1) General Properties of the Ray Tracing Lens

(3.1.1) Conical-wave focusing lenses

(3.1.2) Conical-wave transforming lenses

(3.2) Other Alternative Luneburg Lens Structures

(3.2.1) Uniform Outer Layer Lens

(3.2.2) Two Shell Lens

(3.2.3) Rozendal Lens

(3.3) Conical-Wave focusing Lenses Synthesis

(3.3.1) 2-D Parallel-Plate Lens with TE Mode Propagation

(3.3.2) 2-D Parallel-Plate Lens with TEM Mode Propagation

IV. Liquid Crystal Material Properties

- (4.1) Test Arrangement of Tuneable Patch Element**
- (4.2) Collaboration to Progress Material**
- (4.3) Concept for Tuneable Lens Fabrication**

V. Reflection Amplifier

VI. Conclusions and Future Work

VII. Appendix

- (A) Holey Metal Plate Luneburg Lens operated in TE mode**
- (B) Holey Metal Plate Luneburg Lens operated in TEM mode**

References

List of Symbols, Variables and Acronyms

a: spacing between parallel plates;

Constants in the ray tracing geometry;

b: distance between adjacent holes in holey dielectric material and holey metal plate;

Constants in the ray tracing geometry;

d: diameter of holes in the holey dielectric material and the holey metal plate;

f: frequency;

k: propagation constant in parallel plate region in the holey metal plate structure;

l: length of the simulated parallel plate;

n: refractive index of lens;

r: normalized radius;

t: thickness of the dielectric material used in the holey dielectric lens;

p: variable used to represent the direction of the exit radiation beam in the ray tracing lens;

b_max: max value of b;

d_max: max value of d;

l_x: physical length of the matching layer;

n_x: refractive index of the matching layer;

r0: radius of the lens;

r1: distance from the origin (lens centre) to the focal point;

K: dielectric constant of the material; constant along a ray path;

N: number of the holes in the holey dielectric material;

R: electrical path length in the ray tracing geometry;

S: geometric distance;

Z_{in}: input impedance of the one port reflection amplifier circuit;

Z_s: output impedance of the one port reflection amplifier circuit;

α: departure angle of the ray at focus position;

β: inclination angle in the conical-wave focusing lens;

β0: propagation constant in free space;

γ : inclination angle in the conical-wave transform lens;
 ζ : an auxiliary variable;
 χ : an auxiliary variable;
 $\epsilon(r)$: variable permittivity as the function of r ;
 $\epsilon_{eq}(r)$: equivalent permittivity in the holey dielectric material as a function of normalized radius;
 ϵ_r : permittivity of the holey dielectric material;
 λ : free space wavelength;
 λ_g : guided wavelength;
 λ_1 : new wavelength in the Conical-Wave focusing Lenses Synthesis;
 λ_2 : original wavelength in the Conical-Wave focusing Lenses Synthesis;
 λ_{g0} : original guided wavelength in the holey metal plate when no holes exist;
 λ_{g1} : equivalent guided wavelength in the holey metal plate when holes exist;
 Γ : reflection coefficient;
 θ : total angle including central angle used in ray tracing geometry;
 θ_{3dB} : half power beam width;
 θ_{10dB} : angle at which the power of the feed radiates 10 dB below that of the feed direction;
 Φ : intersecting angle used in the ray tracing geometry;

TE₀₁ mode: in the parallel plate structure, the polarization of the E field is parallel to the plates;

TEM mode: in the parallel plate structure, the polarization of the E field is perpendicular to the plates;

2D: two dimensional;

3D: three dimensional;

LC: liquid crystal;

LCP: Liquid Crystal Polymer;

MDLC: Multilayer Dielectric Liquid Crystal;

PHEMT: Pseudomorphic High Electron Mobility Transistor;

RA: reflection amplifier;

I. Introduction

The Luneburg lens, [1], is a well known device used for wide angle scanning. For land mobile operation, an antenna capable of scanning in a two-dimensional (2D) plane is desirable, especially if the scan angle is large. The Luneburg Lens can be used as a means for creating mechanically scanned beams, single or multiple, at microwave frequencies. However with the advent of phased arrays the lens nowadays tends to be used for radar applications as a wide angle passive reflector.

The objective of this report is to consider if suitable lens configurations can be established which would permit the inclusion of d.c. controllable dielectric material into a Luneburg Lens in order to make the lens capable for electronic scanning. In addition the possibility exists for adding reflection amplifiers along the periphery of the planar lens in order to form an active reflector and thereby enhance its reflection properties. In the work we presented here we concentrate on two-dimensional microwave planar Luneburg lenses for use in the unlicensed 24 GHz ISM vehicular radar telemetry frequency band, [2]. Fig. 1.1 shows the project structure.

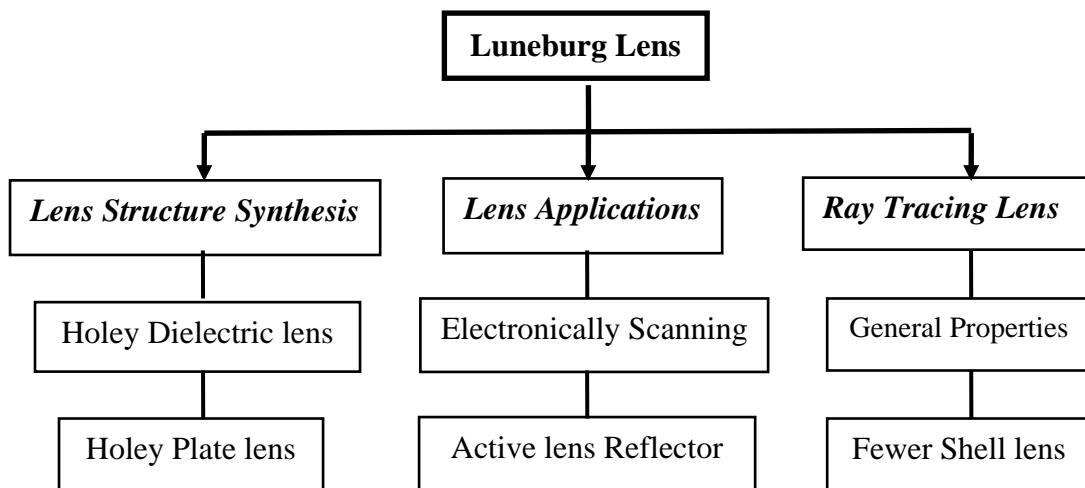


Figure 1.1 Project Structure

Several approaches are evaluated for the synthesis of these 2-D lenses, namely artificial dielectrics are built by drilling holes into a homogeneous dielectric sheet or by etching holes into one of the conductors (metal plates) of a standard PCB material.

The drilled hole method could lead to lens structures that ultimately could be electronically tuned by selectively introducing and biasing liquid crystal (i.e. electronically tuned variable permittivity material) into them. In this report we detail a modified method for improving the control of the permittivity distribution of a dielectric profiled parallel-plate Luneburg lens. Here we use a combination of circular and triangular dispersed equivalent volume-averaged relative permittivity control as well as transverse resonance method guided permittivity thickness control. For verification a prototype lens was designed and measured at 24 GHz, measurement and simulation results show good agreement.

By exploiting holey plate lenses operated in TE_{01} mode or TEM mode propagation, it is shown how standard PCB materials can be used with the potential for low cost lens fabrication, and mass production using photolithographic techniques.

Further, the general properties of the Luneburg-Type Lens are analyzed and a class of lenses which allows the incident EM wave to focus at any required position is presented. The properties of these lenses are parametrically studied in order to investigate the possibility of electronic scanning by the lens. We also investigate the possibility of quantizing the lens permittivity graduation into fewer values so as to facilitate design and fabrication. It is shown that in these situations an additional impedance matching layer is needed in order to rematch the lens to free space.

The preliminary design for a reflection amplifier (RA) is presented based on an OMMIC PHEMT transistor [3] and GaAs MMIC process. The preliminary simulation shows this RA could produce 14 dB Gain when operated at 24 GHz. It is possible to arrange such RAs along the periphery of the planar lens in order to form an active lens reflector so as to enhance the radar cross-section reflection properties of the vehicle on which the lens is mounted.

II. Luneburg Lens Synthesis Techniques

(2.1) Holey Dielectric Lens (Fractional Volume Permittivity Control)

A planar Luneburg Lens whose permittivity distribution is controlled by two types of hole density methodology in the central region and by dielectric thickness control in the edge region is reported. The lens was designed to operate at 24 GHz in TEM mode. Experimental radiation patterns show good agreement with simulated performance. The measured 3 dB beamwidth of the vertical polarized H-plane pattern is 5° with 16.6 dB gain at 24 GHz for a 12.2λ , 15.24 cm diameter lens, cross polar levels were below -30 dB. Its small size and lightweight, 53% of material is removed, and better than 20% bandwidth makes it useful for automotive short-range radar and telemetry equipment. Also, this lens was connected to five impedance matched 3-D tapered microstrip lines arranged with 20° spacing in order to produce multiple beams.

(2.1.1) Permittivity Distribution Control

The permittivity control needed in order to obtain the refractive index

$$n(r) = \sqrt{2 - r^2} \quad (2.1)$$

can be obtained by varying the height for a fixed permittivity material between constant spaced parallel plates, or be keeping the dielectric height constant and grading its dielectric constant. The former approach requires that non-scattering spacers be inserted between upper and lower parallel plates since the height profiled dielectric may not extend to the upper plate; hence the parallel plates need to be supported in a mechanically robust way.

In [4] Sato introduced a 2D permittivity controlled lens. For 10 GHz operation ripples of up to $+\/- 10^\circ$ were observed in the exit plane wave phase distribution. This variation was attributed to dielectric layer discontinuities. From (2.1) the refractive index distribution required for a Luneberg lens is 2 at the center of the lens decreasing to 1 at its periphery. To facilitate construction it would be useful if we could take a fixed permittivity base material whose thickness facilitates the construction of a parallel plate structure whose spacing is less than $\lambda_g/2$ (λ_g is the guided wavelength),

so that only the TEM mode will propagate, and modify its refractive index according to (2.1). The modification required should leave the material with the radial permittivity variation as prescribed in (2.1). In addition the permittivity in any particular region should not exhibit angular dependence. A simple way to obtain this result is to modify the dielectric constant of a constant thickness, constant permittivity material by introducing fractional volume control, i.e. by selective introduction of voids into the material. If cylindrical air holes parallel to the \mathbf{E} vector shown in Fig. 2.1 are introduced then the equivalent volume-averaged relative permittivity technique can be exploited [4-6].

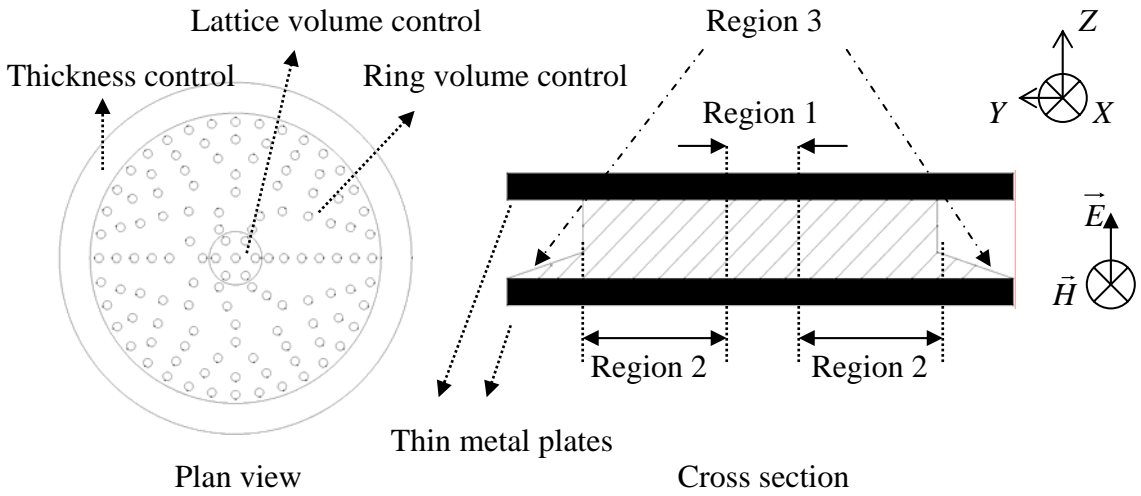


Figure 2.1 Planar Luneburg Lens with the permittivity distribution controlled by hole density and dielectric thickness

In region 2, in order to obtain the required effective relative permittivity N holes of diameter d are drilled along the periphery of a circle of radius r . The resulting effective relative permittivity, $\epsilon_{eq}(r)$ can be estimated by the weighted average of the volume of the holes with a relative permittivity of 1 and the volume of the relative permittivity of ϵ_r , [4], according (2.2):

$$\epsilon_{eq}(r) = \frac{N \cdot \left(\frac{d}{2}\right)^2 + \epsilon_r \cdot \left[\left(r + \frac{d}{2}\right)^2 - \left(r - \frac{d}{2}\right)^2 - N \cdot \left(\frac{d}{2}\right)^2 \right]}{\left(r + \frac{d}{2}\right)^2 - \left(r - \frac{d}{2}\right)^2} \quad (2.2)$$

Using (2.2) the total number of holes N equally spaced around the circumference of a circle of radius r can then be derived in order to realize the required permittivity

distribution of the lens. For hole diameter and adjacent hole spacing less than one tenth and one fifth of a wavelength respectively this method functions well at larger radii and leads to a dielectric which exhibits little angular dependence. This property is important in a Luneburg lens since as a consequence of focussing action ray trajectories at a variety of angles can exist within the lens structure. In addition if the distance to adjacent radii is very small then the permittivity change is relatively smoothly graded with respect to the distance r from the center and minimal discontinuity due to discrete permittivity grading should occur.

In region 1 of the lens where the required permittivity is at its highest, the hole density is small, consequently fewer holes are needed in each ring. This means that the spacing between neighbouring holes are large, which may cause the dielectric to exhibit anisotropic behaviour. To accommodate this, the equilateral triangular lattice arrangement with side length, b , as suggested in [6] is preferred, since it has been shown to give good angular independent characteristics, as well as allowing a larger equivalent permittivity variation for a given d/b ratio than other lattice patterns. The equivalent volume-averaged relative permittivity for the triangular lattice is, [6]:

$$\varepsilon_{\text{eq}}(r) = \varepsilon_r - \frac{2 \cdot \pi}{\sqrt{3}} \cdot \left(\frac{\frac{d}{2}}{b} \right)^2 \cdot (\varepsilon_r - 1) \quad (2.3)$$

Here b is the central distance between the adjacent holes (lattice constant) in this region. Again it is essential that the radius of each hole, $d/2$, and the spacing between neighbouring holes, b , are significantly smaller than the guided wavelength so that the dielectric material appears locally homogeneous.

In region 3 the relative permittivity of the Luneburg Lens approaches 1 at the edge of the lens and the total number of holes must be significantly increased in order to realize the permittivity value needed. As a result, the neighbouring holes will almost certainly contact or overlap, and thus the method of perforating the solid dielectric can no longer be deployed. Therefore in region 3 we use a constant value dielectric material and vary its thickness as a function of lens radius, thus obtaining the permittivity control needed. The transverse resonance method (TRM), [7], yields equation (2.4) which provides the relationship between the dielectric thickness and the

required equivalent permittivity more accurately than the edge control method used in [4], which simply used the ratio of the dielectric thickness and the plate spacing to predict the equivalent permittivity of the lens.

$$\tanh\left[\frac{2 \cdot \pi}{\lambda} \cdot (a - t) \cdot \sqrt{1 - r^2}\right] - \frac{1}{\epsilon_r} \cdot \sqrt{\frac{\epsilon_r - 2 + r^2}{1 - r^2}} \cdot \tan\left(\frac{2 \cdot \pi \cdot t}{\lambda} \cdot \sqrt{\epsilon_r - 2 + r^2}\right) = 0 \quad (2.4)$$

where a is the spacing between the metal plates and t is the thickness of the dielectric.

(2.1.2) Lens Design

For verification, a planar Luneburg lens of 76.2 mm (6.1λ) radius was designed at 24 GHz and fabricated using a 4 mm thick dielectric sheet ($\epsilon_r = 2.54$, $\tan \delta = 0.0005$), [8]. An ideal Luneburg lens with these dimensions should yield a radiation pattern with 4.8° half power beam width and 16.9 dB gain, [9]. Table 2.1 describes the physical positions and permittivity ranges of each of the three regions in the lens. Holes are made using standard 0.5 mm radius (0.04λ) drill bits in both regions 1 and 2.

Region	Physical Range (mm)	Permittivity Range	
(1) lattice volume control	0 ~ 12	2.000	1.975
(2) ring volume control	12 ~ 57	1.975	1.440
(3) thickness control	57 ~ 76.2	1.440	1.000

Table 2.1

In the region 1 the lattice constant b of the triangular pattern holes was selected to be 1.59 mm which represents an equivalent permittivity of 1.988. This is the average of the permittivity values across the region, i.e. 1.975 to 2. The rationale for choosing the average value was that, as can be seen from, Fig. 2.2, the field lines are reasonably parallel in this region. Fig. 2.2 shows the simulated, [10], E field distribution in the X-Y, H- plane when point source excitation is applied at the rim of the lens.

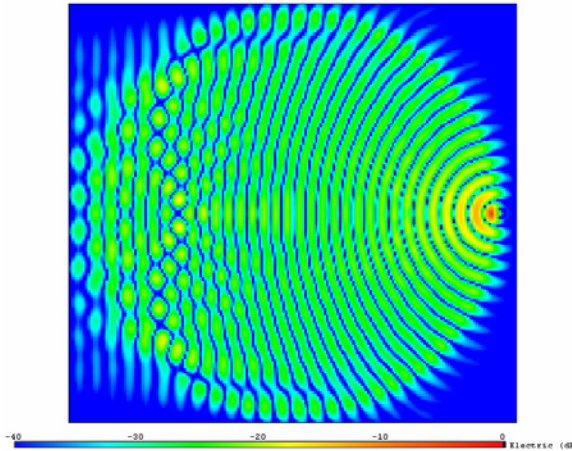


Figure 2.2 Simulated \vec{E} Distributions

Region 2 is quantized into 45 radial steps (radii from 12 mm to 57 mm at 1 mm increments) selected to minimise step change hence permittivity induced discontinuities. The holes are uniformly positioned around the circumference of each circle, with the adjacent spacing greater than 0.1mm. The average spacing between holes in adjacent circles across this region lies is approximately 0.3 mm. Fig. 2.3 shows the equivalent permittivity and the number of holes at each circle radius. The total number of holes in region 2 of the annulus is 6711. The deviation from the required equivalent permittivity across the annulus from the actual required permittivity is no more than 0.01 so that little beam perturbation should occur as a result of radii to radii permittivity discontinuity.

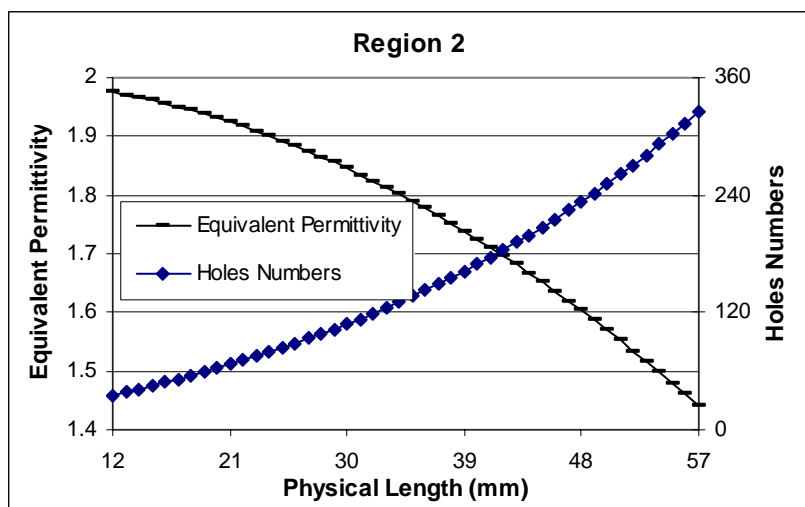


Figure 2.3 The equivalent permittivity variation and the number of holes at each circle of radius r within the 2nd region

Region 3 which lies between 57mm and 76.2mm takes up a radial length of 19.2 mm (1.5λ). The desired permittivity distribution in this region as realized by varying the dielectric thickness from 1.57 mm to 0 mm according to (2.4) is given in Fig. 2.4.

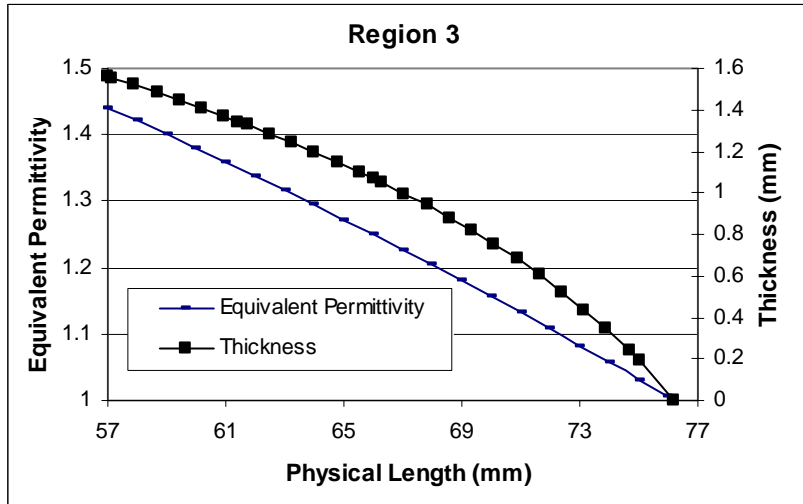


Figure 2.4 The equivalent permittivity variation and the thickness of the dielectric at each radius r within the 3rd region

Fig. 2.5 shows a close up photograph of a segment of the lens in the area of regions 2 and 3, the holes and region 3 profiles are obtained using a CNC machine.

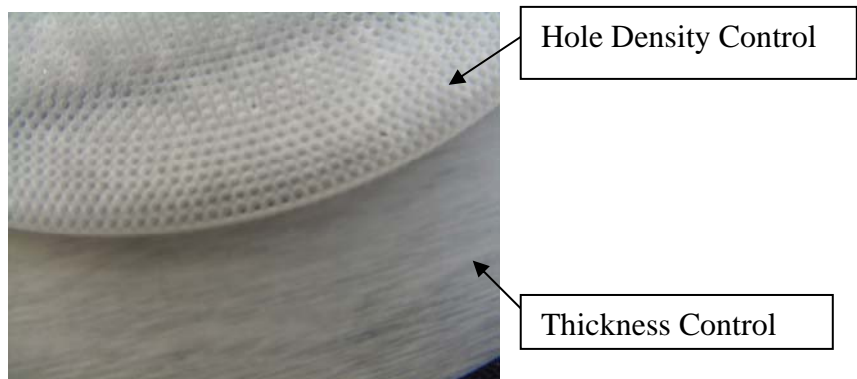


Figure 2.5 Fabricated Lens

(2.1.3) Simulation and Measurement

The lens designed above is simulated using the commercial Micro-Stripes software package [10]. The lens was excited at 24 GHz using a plane wave and an E-field probe positioned at the lens rim was connected to a spectrum analyser. By moving the

E-field probe around the rim of the lens (in both horizontal and vertical polarization orientations) the received signal power was recorded.

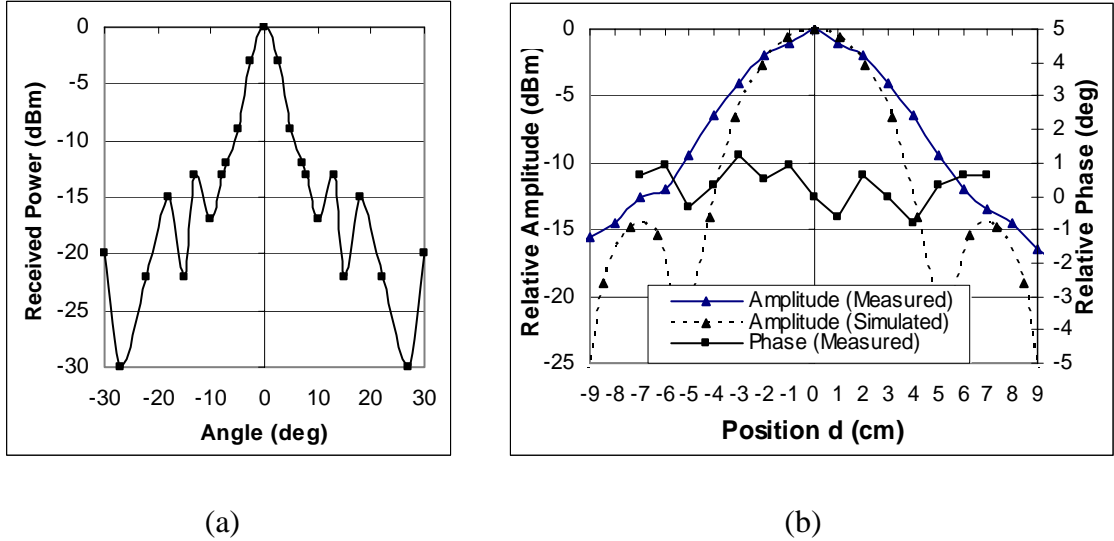


Figure 2.6 Measured co-polar \vec{E} field (a) field distribution along the lens periphery when excited by plane wave; (b) far field pattern with point source excited at lens rim.

Fig. 2.6(a) shows the measured \vec{E} field pattern in the X-Y, H-plane of the lens; the measured cross polar level was below -30 dB. The 3 dB, HPBW, measured beamwidth of the focused spot is about 5° , c.f. the predicted value of 4.8° , and simulated value of 4.1° at 24 GHz. Simulated and measured lens gains were 16.73 dB and 16.6 dB, respectively, c.f. the theoretical effective aperture based calculation, [9], of 16.9 dB. Fig. 2.6(b) shows the measured phase variation across the radiated wave front. This is plotted relative to the zero degree position using an E-field probe moved along an 18 cm long tangent positioned diametrically opposite to the point source position and along the boresight direction at a distance of 20λ from the lens rim. From this result it can be seen that the cylindrical wave radiated from the monopole is converted to a plane wave since the phase ripple is less than $\pm 1^\circ$. In [4] which used only region 2 controls and an approximate edge control method for region 1 gave for a 10λ lens, 13.2 dB gain, operating at 10 GHz $\pm 10^\circ$ phase ripple. This comparison suggests that the three region control methodology used in this paper is superior to previous approaches which use less sophisticated permittivity grading methodologies.

The recent European Commission Decision, [11], now permits the frequency band from 21.65 GHz to 26.65 GHz to be used for vehicular radar/telemetry systems. Thus we tested the lens over this band of frequencies, the results are summarised in Table 2.2.

Frequency (GHz)	21.65	24	26.65
Aperture Electrical Size (λ)	11	12.2	13.5
HPBW (deg)	Theoretical	5.3	4.8
	Simulated	4.4	4.1
			3.8

Table 2.2

Since the dimensions of the holes are still significantly small over this frequency range the holey dielectric material appears locally homogeneous and is remains useful over the required 20% bandwidth. At the band edges the measured co-polar response agrees with simulation and cross polar levels are better than -30 dB. It is noted that the simulated HPBW is less than the theoretical value calculated from [9] which is most accurate for lens apertures larger than 14λ , while the lens here has an aperture range of 11λ to 13.5λ .

(2.1.4) Lens with 3-D Tapered Microstrip lines

In order to provide the possibility for transmitting or for receiving multiple beams, the lens above is connected to impedance matched 3-D microstrip line tapers. 3-D tapered lines were designed using Taconic TLY 5A, (standard thickness of 0.508 mm, $\epsilon_r=2.17$) [17]. From the measured field distribution alone the lens periphery (Fig. 2.6(a)), θ_{3dB} and θ_{10dB} was estimated to be 5° and 12° , respectively. So the input impedance at the lens periphery was assumed to be that of a microstrip line with 5° radial width (6.65 mm) and lens height (4 mm). This impedance was obtained from Microstripes [10] to be 98.2Ω and it was tapered to 50Ω using both height and line width control. In total we estimate that 5 microstrip lines could be arranged around the lens rim of 90 degrees section with 20° between each line since at this point the field maxima has dropped to -18 dB. A simulated return loss of -20 dB at 24 GHz was obtained. Fig. 2.7 shows the taper geometry and dimensions used.

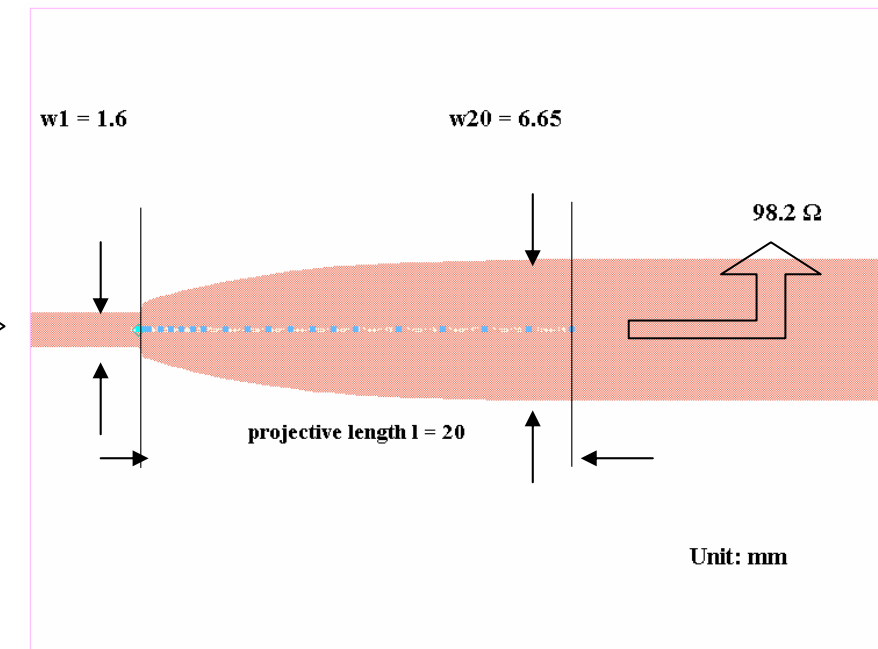
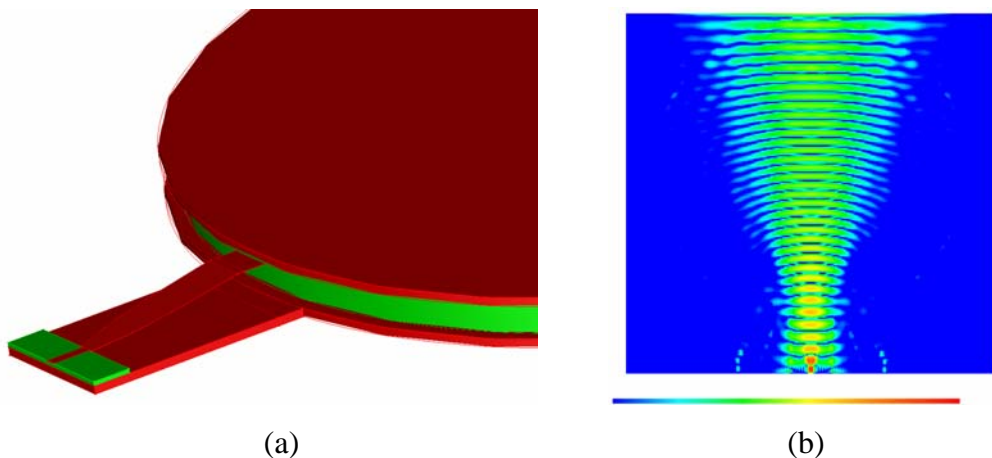


Figure 2.7 Taper geometry and dimensions

Fig. 2.8 (a) shows the partial simulated geometry of the lens with one 3-D taper; (b) is the simulated field distribution of the lens when connected to five adjacent tapered lines and excited by a series of diametrically positioned plane waves; it is clear that the port to port isolation is estimated to be -30 dB; (c) shows that the simulated and measured S21 coupling between the adjacent tapered ports at 24 GHz is -28 dB and -34 dB, respectively; the coupling is smaller than – 40 dB when ports' adjacent angle is larger than 20 degrees; (d) is the predicted far field pattern which clearly shows multiple beam formation. Each coloured curve represents each excitation direction.



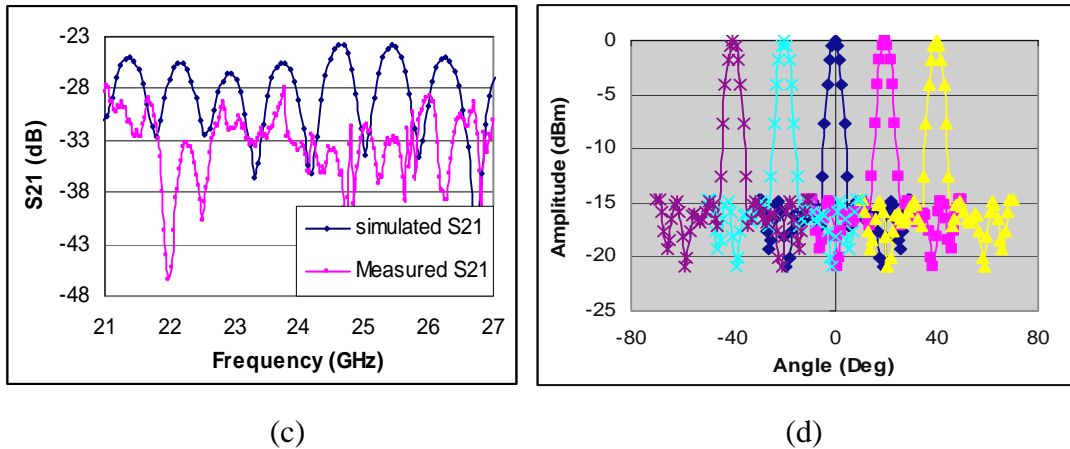


Figure 2.8 Lens with 3-D Taper microstrip line illuminations

The overall length of the taper is 20 mm (1.6λ), with an inclined angle of 9.9° with the horizontal plane. The PCB was fabricated by LPKF milling [12] of the dielectric and then bent into the required angle to be connected with the lens periphery.

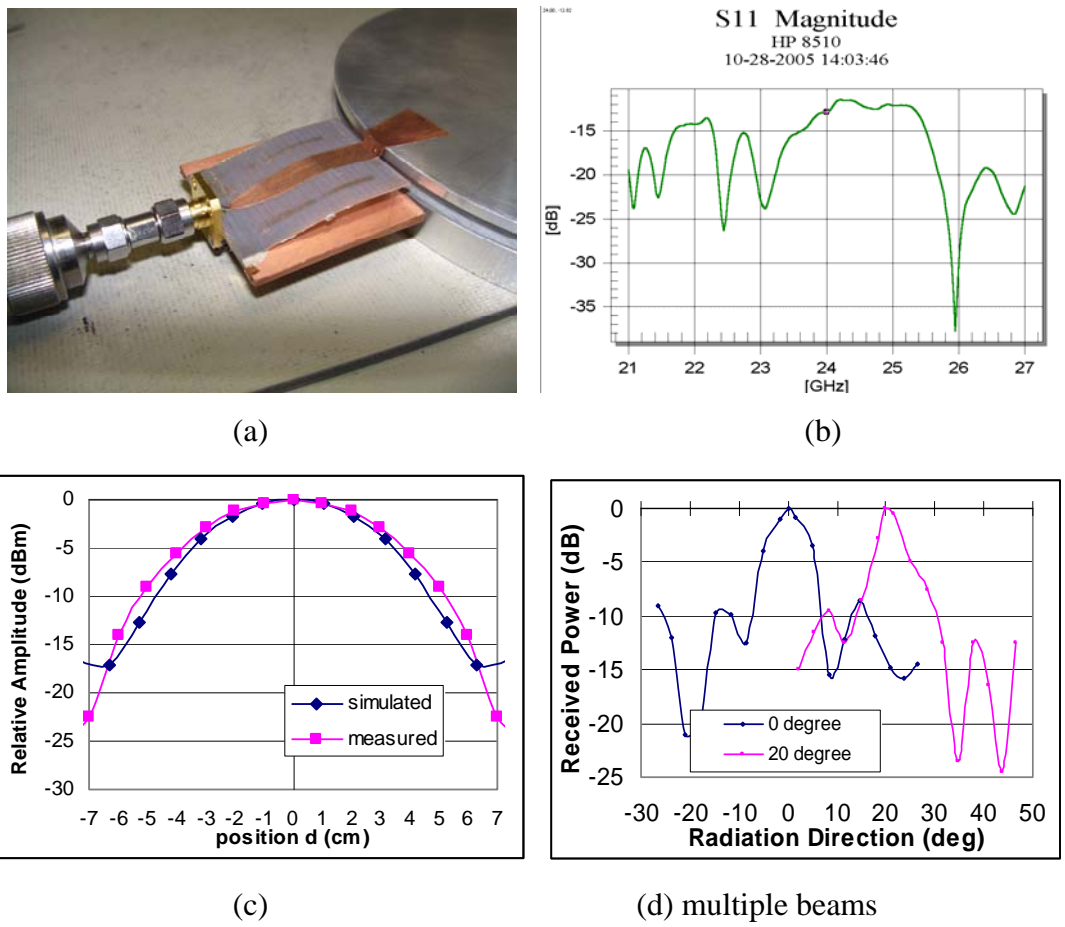


Figure 2.9 Measured microstrip line excited lens

Fig. 2.9 (a) is the photo of the Taper with lens under measurement. The measured return loss of the excitation port (S11) was -12.82 dB at 24 GHz, and over the bandwidth [11] from 21.65 GHz to 26.65 GHz it was shown in Fig. 2.9 (b). Fig. 2.9 (c) shows the simulated and the measured results of co-polar \vec{E} field radiation pattern which is plotted relative to the zero degree position using an \vec{E} field probe moved along a 14 cm long tangent positioned diametrically opposite to the point source position and along the boresight direction at a distance of 40λ from the lens rim. These two patterns are in good agreement. The measured θ_{3dB} for microstrip excitation is 5° which is slightly larger than that of the lens excited by a point source ($\theta_{3dB} = 4.1^\circ$); (d) is the measured co-polar far field radiation pattern of the lens when excited by two ports placed with a 20 degree angular separation between them. The measured cross polar level was better than 25 dB below that of the co-polar in all cases.

Summary Conclusions 2.1

It has been demonstrated that by combining three different volume control strategies for spatially grading the refractive index of a constant thickness fixed permittivity dielectric slab that excellent lens performance can be obtained. The lens designed here is compact and is lightweight since about 53% of the dielectric material has been removed. The lens has excellent focusing performance and high gain over 20% bandwidth. Such a lens could find application in multiple beams forming or scanned beam antennas for land mobile vehicular radar and telemetry use, or in applications where increased radar return from vehicles is required.

(2.2) Holey Plate Lens

The holey plate is another possibility for planar Luneburg Lens construction. This structure could facilitate fabrication since in principle by photo lithographically etching holes into one side of a standard PCB we can introduce inductance which can be used to partially neutralise the permittivity of the material in a localised region, i.e. give permittivity control.

(2.2.1) Holey Metal Plate Luneburg Lens Operated in TE mode

A dielectric filled parallel holey metal plate with TE_{01} mode propagation could in principle be used in Luneburg Lens applications since this structure is capable of providing a refractive index from nearly zero to a value approaching the square root of the dielectric between the plates [13~14]. This method relies on the principle that a leaky waveguide, one with holes drilled in its narrow wall, could yield variation of equivalent refractive index, [15~16]. The advantage is that it would give a manufacturing strategy that would remove the necessity to drill dielectric since by using standard microwave PCB material we could fabricate the lens by etching holes into one of the PCB ground planes. This approach if viable would also offer the prospect of producing very low profile lenses, which have the potential for easier introduction of liquid crystal material than the fractional index controlled lenses described above.

In order to check the validity of the master design equation (2.5), given below, [13], a model lens is simulated at 24GHz for operation under TE_{01} ($a = 5\text{mm}$) mode propagation; Fig. 2.10 shows the conceptual of the model structure.

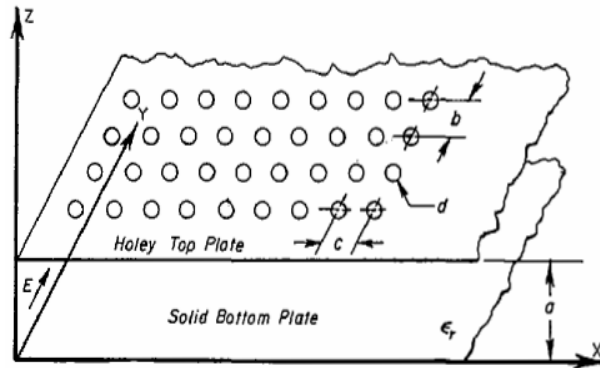


Figure 2.10 Holey Metal Plate Lens with TE_{01} Mode [13]

From simulation, we find that:

- (i) the phase shifts of S_{21} agree with those of the equation and that by correct choice of hole size and spacing that effective permittivity can be adjusted;
- (ii) The magnitude of S_{11} is almost 0 and S_{21} is almost 1, respectively. So most of the energy will propagate through the plates, i.e. there is little energy lost by leakage;

Thus this method could be used to vary the refraction index so as to build the lens.

(1) Range of Parameters Required for Luneburg Lens Application

In Luneburg Lens application, the refraction index n varies from 1 to $\sqrt{2}$. So the variation is $\sqrt{2} - 1 \approx 0.414$; the frequency is $f = 24$ GHz, $\lambda = 12.5$ mm; see (2.5) below, λ_{g0} is the original guided wavelength in the holey metal plate when no holes exist; λ_{g1} is the equivalent guided wavelength in the holey metal plate when holes exist; $n(b)$ is the final equivalent refractive index:

$$\begin{aligned}
 \beta_0 &= \frac{2\pi}{\lambda} & k &= \frac{2\pi}{a} & \lambda_{g0} &= \frac{\lambda}{\sqrt{\epsilon_r - \left(\frac{\lambda}{2a}\right)^2}} \\
 G(b) &= \frac{b}{2k} \left[k^2 - (\epsilon_r - 1) \cdot \beta_0^2 \right] & B(b) &= \frac{6b \cdot b}{k \cdot d^3} & X(b) &= \frac{B(b)}{B(b)^2 + G(b)^2} \\
 \lambda_{g1}(b) &= \frac{\lambda_{g0}}{1 + \frac{\lambda_{g0}^2 \cdot X(b)}{4\pi \cdot a^2}} & n(b) &= \frac{\lambda}{\lambda_{g1}(b)} & & (2.5)
 \end{aligned}$$

There are four variables we could change to get the required refractive index n : these are ϵ , a , b and d ;

ϵ is the permittivity of the dielectric material;

a is the spacing between the two plates; $a > \lambda / (2\sqrt{\epsilon_r})$;

b is the spacing between the neighbouring holes; $b < \lambda / (2\sqrt{\epsilon_r})$;

d is the diameter of the holes; $d < b$;

Based on the equation, the d and n are in direct proportion, so at the rim of the lens, in order to facilitate the construction, the spacing between the two plates, a , is first adjusted to make $n = 1$. Thus no holes will be required on the metal plates in the outer region.

$$a = \frac{\lambda}{2\sqrt{\epsilon_r - 1}} \quad (2.6)$$

Other values for a exist but are not preferred since:

- (i) If a is larger than the value needed to make $n = 1$, i.e. n is larger than 1 at the rim, the method is rendered useless as holey metal plates can only increase the value of n from its value in a solid plate structure.

(ii) If a is smaller than the value needed to make $n = 1$, i.e. n is smaller than 1 at the rim, the variation range of n has to be increased, i.e. the number of the holes are increased.

Also b and n occur in inverse proportions, while d and n occur in direct proportions. However d can produce much larger variation than b , so d is the key design factor here, i.e. we could fix b and get the required n by changing d . In this case, the lens will be an equal height dielectric filled parallel plate structure with small holes in the outer regions of the upper plate and larger holes in the central region. In the design process for (2.5) to remain valid, b_{\max} (the max value of b) is set to be $\lambda / (2 * \sqrt{\epsilon_r})$, while d_{\max} (max value of d) is set as $0.8 * b$ in order to minimise leakage energy.

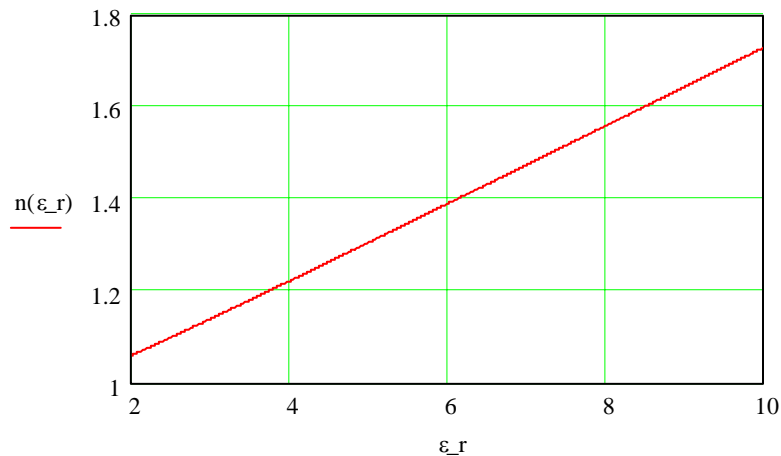


Figure 2.11 Max available refractive index

Fig. 2.11 shows the maximum equivalent refractive index this holey plate could achieve by this method for different permittivity PCB material, i.e. with a required equivalent refractive index of 1.5 for example, the smallest dielectric constant of the PCB substrate is 7.312 under this method. It is apparent that if we start with a small dielectric constant base material we can only get a small refractive index variation. Thus the base dielectric material required for Luneberg lens applications at 24 GHz is about 6.3. Even larger permittivity material is preferred, since larger variation of n would facilitate the fabrication process.

(2) Holey Plate Lens Based on Standard Material (Taconic CER 10, [17])

The standard thicknesses PCB (Cer10, $K=10$) are considered. See from Table 2.3, the frequencies here are computed using (2.6) to make the refraction index equal to 1 for corresponding thickness and K material with TE_{01} mode propagation.

Thickness (mm)	K (dielectric constant)	frequency (GHz)
0.64	9.5	80.390
0.76	9.7	66.914
1.19	9.8	42.492
1.27	9.8	39.815
1.58	10	31.646
1.91	10	26.178
2.54	10	19.685
3.18	10.2	15.551

Table 2.3

When the substrate is thin, the corresponding frequency is so high that it is difficult to find a proper horn antenna to excite the lens, so a thicker material, $\epsilon_r = 10$, $a = 2.54$ mm was chosen. When $f = 19.685$ GHz, the refraction index n is 1 for TE_{01} mode excitation. $b_{\max} = 2.409$ mm.

b (mm)	d	n
2.4	0.8b	1.72
	0.2b	1.01
1.4	0.8b	1.42
	0.2b	1.006

Table 2.4

Table 2.4 shows that, when the b is chosen to be constant, 1.4 mm for example, and d is varied between 0.2 b to 0.8 b , the equivalent refractive index varies from 1 to 1.42, which is suitable for Luneburg lens requirement provided we operate at 19.685 GHz. Detailed design data is presented in Appendix A.

(2.2.2) Holey Metal Plate Luneburg Lens operated in TEM mode

When the plate spacing is smaller than half of the guided wavelength, only the TEM mode can propagate through the parallel plates with holes etched on one side. Here

the electric field is perpendicular to the plates, i.e. we could excite the lens using a microstrip feed to facilitate the fabrication. The hole parameters required for this approach have been investigated using numerical simulation since equation (2.5) is no longer valid for this mode of excitation. See Fig. 2.12. (Data attached in Appendix B).

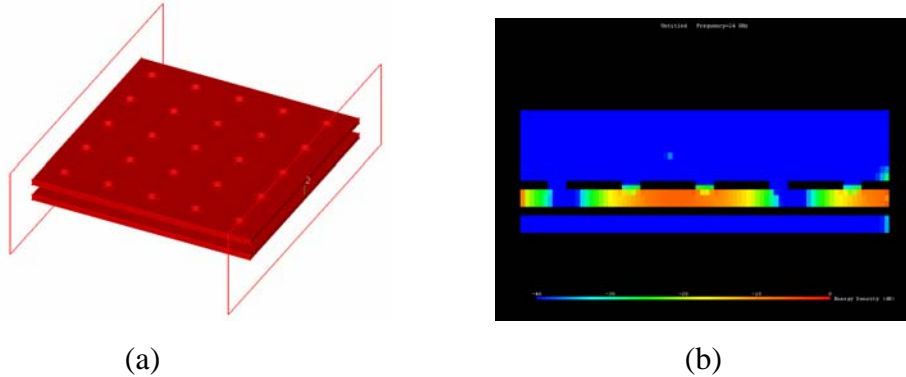


Figure 2.12 (a) Simulation geometry for holey-plate; (b) Energy Density in the cross-sectional view.

The introduction of holes should lead to the phase shift of S21 increasing, which means that the equivalent guide wavelength is reduced, i.e. the refractive index is increased. In the Luneburg Lens, the required refractive index is between 1 and $\sqrt{2}$, which in turn means that the guide wavelengths need to drop from 12.5 mm to 8.839 mm. However, based on simulation, the variation of the equivalent wavelength we can obtain for reasonable hole ranges is too small (from 12.5 mm to 11.8 mm). Thus modifications are needed to improve the performance.

Based on simulation, it is found that small plate spacing and holing both sides of the plates are effective methods to increase the refractive index variation, here the refractive index can be made go up to 1.292. Although it still does not reach the required value ($\sqrt{2}$), according to the derivation of the Luneburg type Lens for focussing onto the lens periphery, it could be used in the design of a lens with focal point at $1.3 r_0$, where r_0 is the radius of the lens. Table 2.5 shows the focusing position of the lens with 0.8 mm diameter holes and 1 mm holes spacing for different plate spacing and holes sides, r_1 is the distance from origin (lens centre) to the focal point.

structure	n	focus position (r_1/r_0)
$a = 0.5\text{mm}$	1.059	5.56

$a = 0.2\text{mm}$	1.15	2.3
$a = 0.2\text{mm} \text{ & both side}$	1.302	1.26

Table 2.5

Next we investigated a parallel-plate which is partially filled with low permittivity dielectric and which can produce an equivalent permittivity of nearly 1.

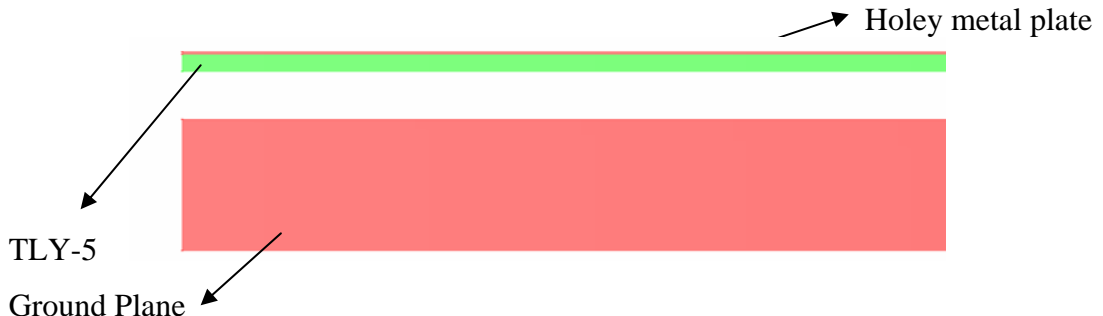


Figure 2.13 Simulated TLY_TEM Holey Lens

From Fig. 2.13 above, Taconic TLY-5, [17] ($\epsilon_r = 2.2$, $\tan \delta = 0.0009$, standard dielectric thickness: 0.13 mm, copper thickness: 0.018 mm) was used with the lower copper removed. The red colour represents metal, the green is dielectric. Here non-scattering spacers are required to be inserted between the upper PCB and the lower ground plane in order to support the suspended part. The distance between the ground plane and the upper plate is 0.5 mm. According to the Transverse Resonance Method (TRM), the equivalent permittivity is 1.08 in this case. Parametric simulation shows that for the $d=0.8\text{ mm}$ & $b=1\text{ mm}$ case, that the focal point will lie at $1.57 r_0$, which is much nearer to the lens periphery than the case of no dielectric ($2.3 r_0$). This means that this type of structure leads to more flexible lens design potential.

Future work will be focused on the preliminary experiments required for verification.

III. Ray Tracing Lens

(3.1) General Properties of the Ray Tracing Lens

The general theory which is applicable to the design of lenses with cylindrical or spherical symmetry was studied, [18~19]. Many of the previously described lens designs are the special cases of the general theory.

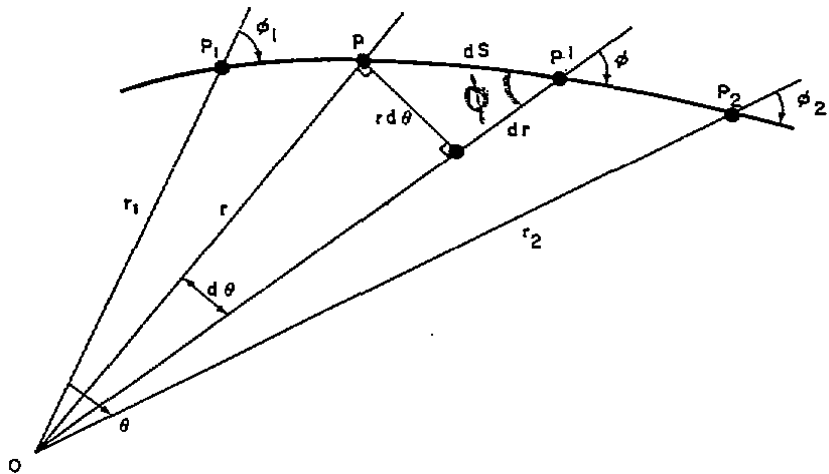


Figure 3.1 Ray tracing geometry [19]

Fig. 3.1 shows the section of a ray which propagates from P1 to P2. The point o is the origin of the polar coordinate system. The ray intersects the polar radius r at an angle Φ . The infinitesimal electrical path length dR is simply expressed in terms of the geometric distance dS :

$$dR = dS = \frac{n \cdot dr}{\cos(\phi)} = \frac{n \cdot r \cdot d(\theta)}{\sin(\phi)} \quad (3.1)$$

The total electrical path length R between the fixed points P1 and P2 has to satisfy Fermat's principle, which leads to the well known condition in terms of the index of refraction $n(r)$ and the angle Φ :

$$K = n \cdot r \cdot \sin(\phi) \quad (3.2)$$

(3.2) can be used to eliminate Φ from (3.1). Integration of (3.1) leads to an expression for the electrical path length:

$$R = \int_{r1}^{r2} \frac{n}{\cos(\phi)} dr \quad (3.3)$$

A similar expression is derived for the total included angle θ as viewed from the origin:

$$\theta = \int_{r1}^{r2} 1 d\theta = \int_{r1}^{r2} \frac{\tan(\phi)}{r} dr = K \cdot \int_{r1}^{r2} \frac{1}{r \sqrt{(n \cdot r)^2 - K^2}} dr \quad (3.4)$$

(3.3) and (3.4) will be the basic forms on which further developments will be built.

Now, let's consider a plane wave impinging on the spherical or cylindrical lens from the left side, as shown in Fig. 3.2. For convenience, the radius of the lens is defined to have unit length. Furthermore, it is assumed that the lens has a dielectric constant at the boundary which equals the dielectric constant of the surrounding medium.

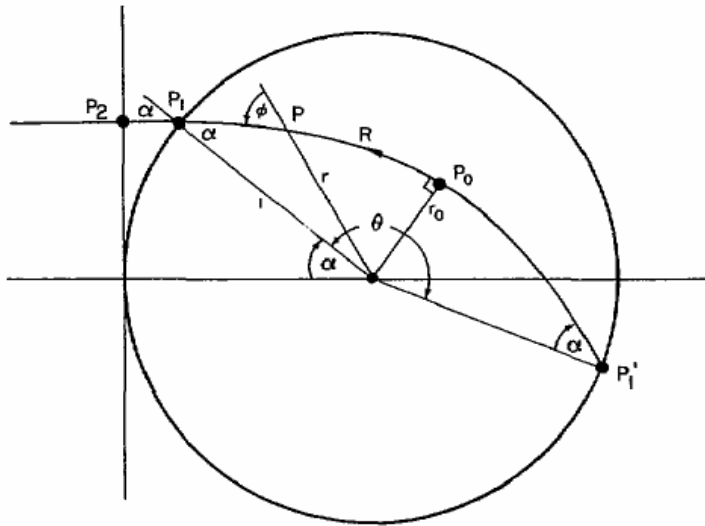


Figure 3.2 Generalized lens cases [19]

In Fig. 3.2, a ray path is shown inside the lens. At P_1 , the ray emerges into the surrounding medium and, because of the matched condition, no discontinuity in the slope of the ray path occurs. Furthermore, because of symmetry and smoothness, there will exist a point P_0 for which the slope $dr / d\theta = 0$. Point P_0 will be the midpoint of the total path P_1 and P_1' . The properties of the lens are defined, if the total path length R from P_1 to P_1' and the total central angle θ are known.

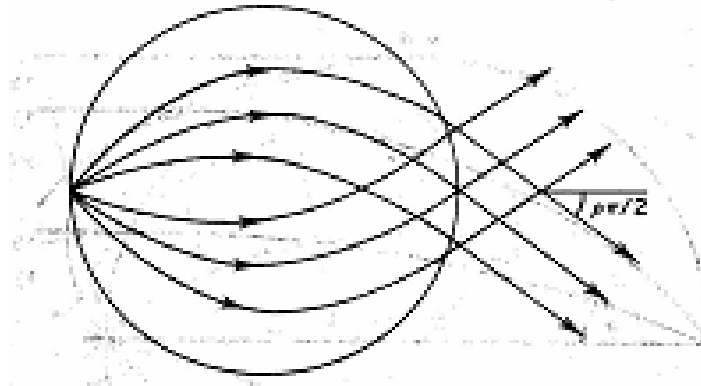


Figure 3.3 Beam separations from point source [18]

Fig. 3.3 is the general case of the ray from the source on the unit circle separated into two beams which have an angle of $(p^*\pi/2)$ with the symmetrical axis. On the contrary, when the lens is excited by a plane wave, the wave will also be separated into two parts, and finally be focused at two points $(p^*\pi/2)$ departing from the point which is diametrically opposite of the incident wave.

This means a class of Luneburg Lens could be produced with either the direction of the radiating beams (point source excitation) or the position of the focusing points (plane wave excitation) rotated along the periphery of the lens. Only when $p = 0$, will the two radiating beam or the two focus points coincide.

The equation for path length R and angle θ for the part of the ray inside the lens are given by the following two equations:

$$R = 2 \cdot \int_{r_0}^1 \frac{n^2 \cdot r}{\sqrt{(n \cdot r)^2 - K^2}} dr \quad (3.5)$$

$$\theta = 2 \cdot K \cdot \int_{r_0}^1 \frac{1}{r \cdot \sqrt{(n \cdot r)^2 - K^2}} dr \quad (3.6)$$

In these equations, K is a constant which depends only on the departure angle α .

Generalize from the (3.2),

$$K = (n \cdot r \cdot \sin(\phi)) = \sin(\alpha) = n \cdot r \cdot c \quad (3.7)$$

In (3.7), $n\theta$ and $r\theta$ are the quantities at point P0, while $\sin(\alpha)$ is obtained from the observation that $n = 1$ and $r = 1$ at the periphery of the lens, and also $\Phi = \alpha$. (Φ is the angle the ray path makes with the radius vector, and α is this angle at the boundary).

In order to bring the two integrals in (3.5) and (3.6) into standard form, two new variables ζ and χ are introduced:

$$(n \cdot r)^2 = 1 - \zeta^2 \quad (3.8)$$

$$\chi = \cos(\alpha) \quad (3.9)$$

At this stage, the value $n(r)$ is unknown, and the purpose of the analysis will be to obtain this function from the known desired values for the path length and central angle. Now, introduce a new function:

$$2 \cdot n^2 \cdot r \cdot dr = -\phi(\zeta) \cdot d\zeta \quad (3.10)$$

Substitution of (3.8), (3.9) and (3.10) into (3.5) and (3.6) leads to the following two fundamental expressions:

$$R = \int_0^\chi \frac{\phi(\zeta)}{\sqrt{\chi^3 - \zeta^2}} d\zeta \quad (3.11)$$

$$\theta = \sqrt{1 - \chi^2} \cdot \int_0^\chi \frac{\phi(\zeta)}{(1 - \zeta^2) \cdot \sqrt{\chi^3 - \zeta^2}} d\zeta \quad (3.12)$$

For $\phi(\zeta)$ in the (3.11) and (3.12), choose a linear function:

$$\phi(\zeta) = a + b \cdot \zeta \quad (3.13)$$

where a and b are constants.

The following relationships are obtained from integration by substitution of (3.13) into (3.11) and (3.12):

$$R = \frac{\pi}{2} \cdot a + b \cdot \cos(\alpha) \quad (3.14)$$

$$\theta = \frac{\pi}{2} \cdot (a + b) - b \cdot \alpha \quad (3.15)$$

$$r^4 = (1 - \zeta)^{a+b} \cdot (1 + \zeta)^{-a-b} \quad (3.16)$$

These equations together define a large class of Lenses with interesting properties. For each value of a and b , a member of the class of lenses is selected. Given the constants a and b , the index of refraction $n(r)$ can be found either directly by elimination of ζ from (3.16) and (3.8) or numerically by using ζ as a parameter between $n(\zeta)$ and $r(\zeta)$. For example, $a = 1$ and $b = 1$ leads to the solution of the standard Luneburg Lens.

Two class of Luneburg-Type lens are now considered:

(3.1.1) Conical-wave focusing lenses [19]

Substitution in Equ.3.14 the value $b = 1$. This class of lenses is characterized by the fact that the ray path equals a constant plus $\cos(\alpha)$. It was found from Fig. 3.2 that the $\cos(\alpha)$ term appears from that part of the ray which passes from the wave front through the surrounding medium before it hits the lens. This property defines a class of lenses which transforms a plane or conical incoming wave into a point focus, where the point focus is located at the periphery of the lens. The value of a determines the cone angle of the incoming wave: $a = 1 - (2\beta/\pi)$. See Fig. 3.4, [19].

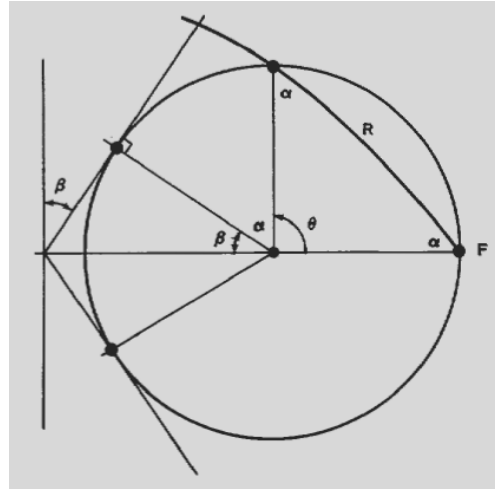


Figure 3.4 Conical-wave focusing lens

For $\beta = 0^\circ$, the standard Luneburg lens is obtained; for $\beta = 90^\circ$, a point radiator placed at the focus of the lens will generate a cylindrical wave. Fig. 3.5, [19] shows plots of dielectric constant versus radius for various values of the cone inclination angle β .

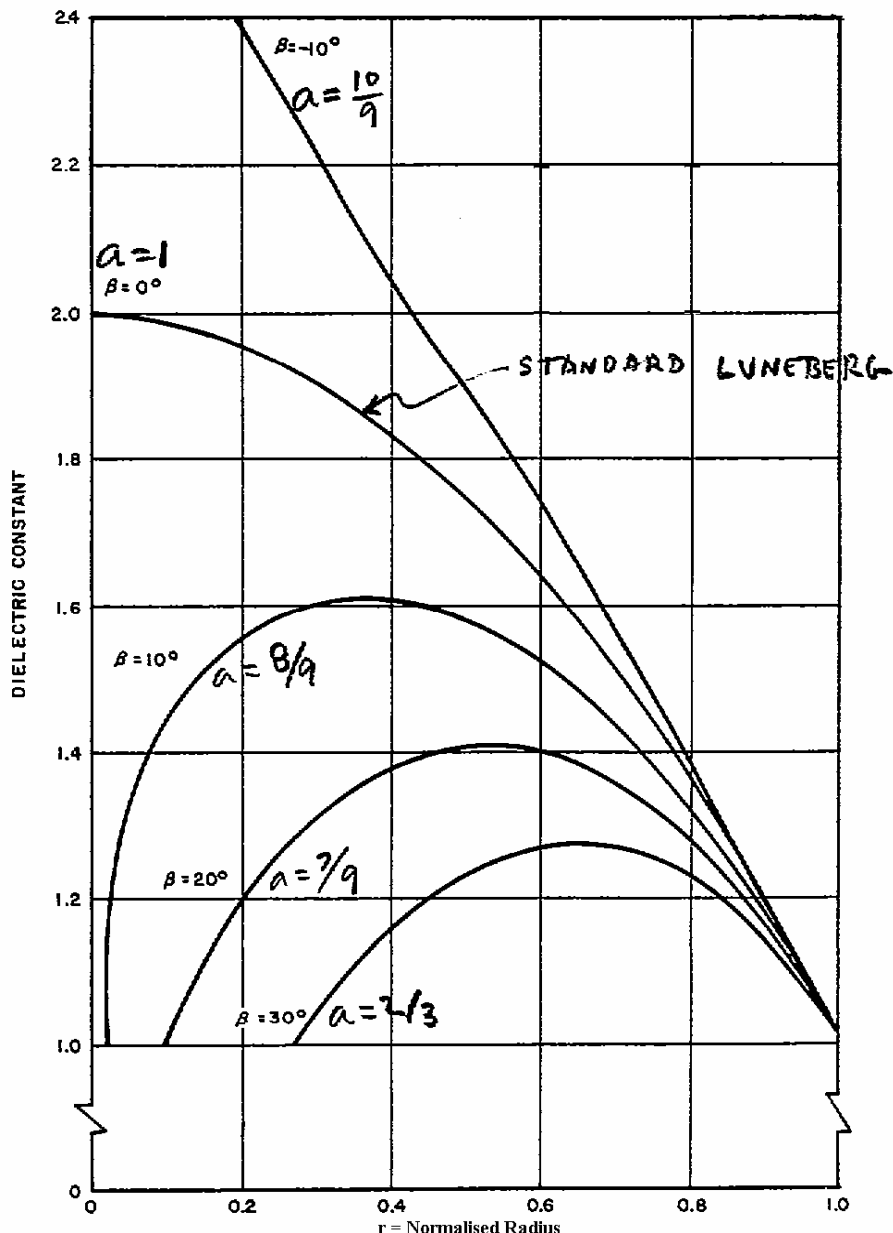


Figure 3.5 Conical wave focusing lens curves

The dielectric filled parallel plate with permittivity of 2.54 and 10 graded steps excited for TE_{01} mode propagation has been used as the structure here in simulation in order to verify the validity of this theory. Plane wave excitation propagation is from left to right (Fig. 3.6); here the energy is focused at the positions $\pm \beta$ degrees to the point diametrically opposite the incident direction. Fig. 3.6 (a) is the E-Field Energy of the case $\beta = -5^\circ$. (b) is $\beta = -30^\circ$. *This methodology suggests the possibility of making a multiple beam sum difference transmit antenna for deployment in for example a monopulse system.*

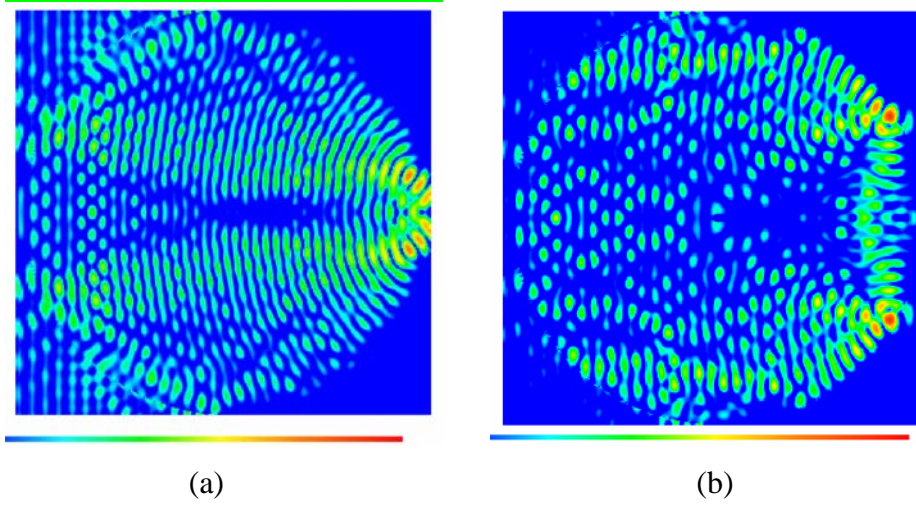


Figure 3.6 Simulated Conical Wave Lens

In section 3.3, this class of the lenses will be synthesized with the parallel plate structure in order to make the radiating beam electronically scanning.

(3.1.2) *Conical-wave transforming lenses*, [19]

This class of lenses is obtained by choosing $b = 2$ in the linear relation. This class has the property of transforming a conical wave with an inclined angle of β into a conical wave with an inclined angle of γ . *This class of lens could have important applications as a Radar Beacon.*

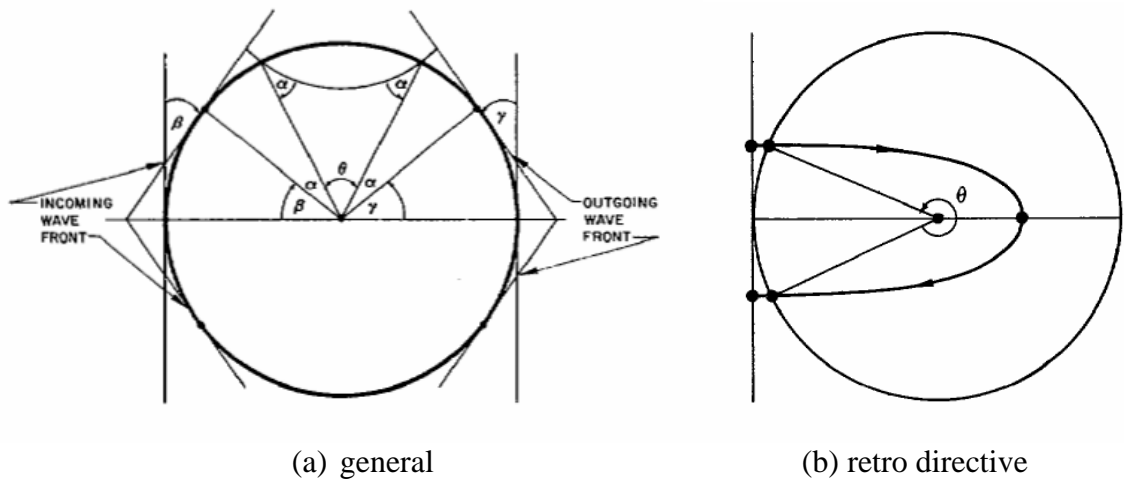


Figure 3.7 Conical-wave transforming lenses [19]

For this type of lens, the constant a is easily expressed in terms of the inclination angles β and γ of the conical waves: $a = -2*(\beta + \gamma)/\pi$. Fig 3.7 (a) is the general case of

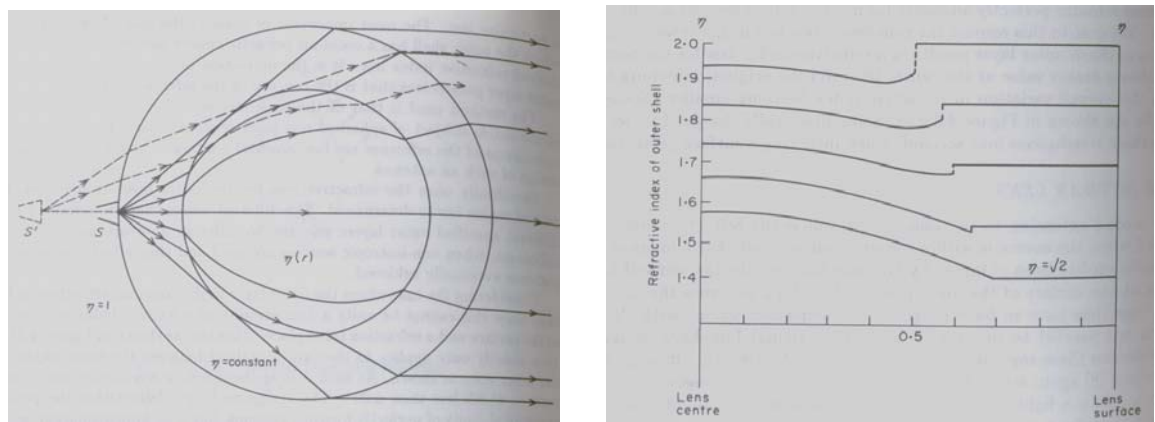
the conical-wave transforming lens; (b) is the special case when $\beta = 0^\circ$, $\gamma = -180^\circ$ (retro directive).

(3.2) Other Alternative Luneburg Lens Structures

All the lens discussed thus far have the property of continuity of direction of the ray path at the boundary of the lens, i.e., the dielectric constant at the outside periphery of the lens matches the dielectric constant of the environment, namely air. Now, the theory will be applied equally to the non-matched condition at the boundary, and may incorporate discontinuity of dielectric constant between material layers. As a result the amount of permittivity grading required is reduced but an impedance matching layer is needed in order to reduce reflection at the lens periphery.

(3.2.1) Uniform Outer Layer Lens [18]

A fundamental extension to Luneburg's analysis has been made by Morgan, who extended the original analysis of Luneburg to permit a refractive index law that is piecewise continuous. Here a spherical Luneburg lens is constructed of shells within in each of which the refractive index follows a particular law. The outer shell has a constant refractive index and the core follows a prescribed refractive index law. Then since this cannot be unity, a discontinuity in refractive index now occurs at the surface and a mismatch occurs. This lens as shown in Fig. 3.8 (a) strictly only applies to the rays contained between the rays tangent to the inner core as shown. As such it is applicable to a microwave source with pattern width less than $\pm 90^\circ$. It is apparent from Fig. 3.8 (b) that the uniform outer layer results in a refractive index law for the central core that has a higher value at the center than did the original Luneburg lens, but that the overall variation in refractive index becomes smaller.



(a)

(b)

Figure 3.8 Uniform outer Layer lens, [18]**(3.2.2) Two Shell Lens [20]**

From the analysis of the uniform outer layer lens above, it is found that the higher the value of $n1$ (the refractive index of the outer region in the lens), the smaller is the variation of $n2$ (the refractive index of the central region in the lens), as a function of the radial coordinate r . Thus by using a very high value of $n1$ it might be possible to find a very good approximation to a perfect lens, even with a constant $n2$. Toraldo has worked out the values for these two shell lens, [20]. His lens consists of a sphere of unit radius, with $n1=3.6$, $n2=2.75$, and the radius of the core $r=0.3863$, see Fig. 3.9. Such a lens would collimate the rays from a point source located on its surface with a maximum angular error of only 2 min of arc up to a diameter of the beam equal to 0.9 times the diameter of the whole sphere. However because of the discontinuity of the refractive index at the periphery surface coatings are needed to reduce the otherwise large loss by reflection associated with this lens.

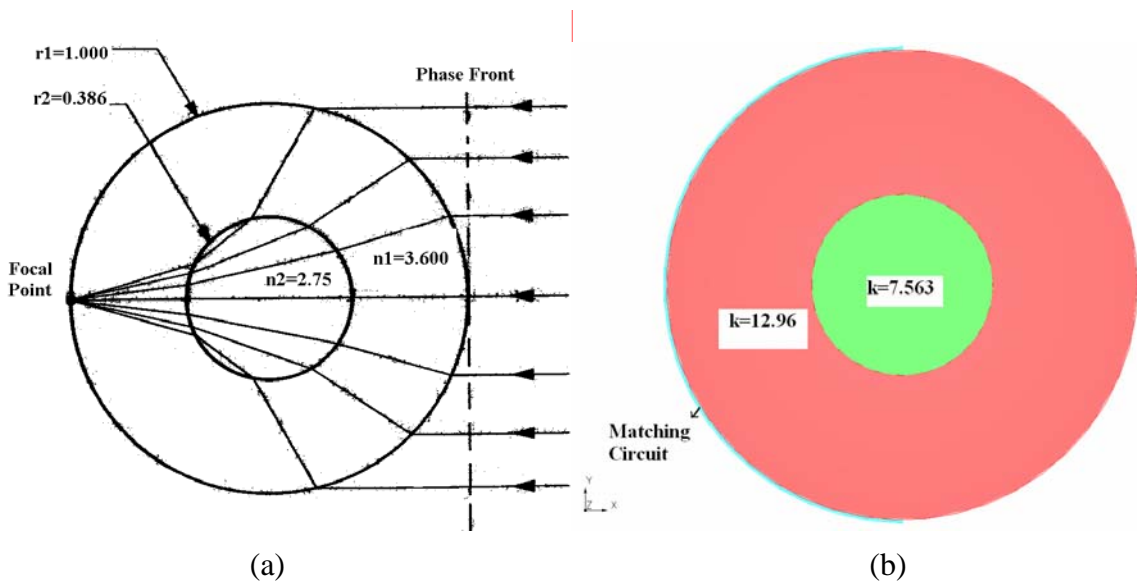
**Figure 3.9 Two Shell lens**

Fig. 3.9 (b) is the simulated lens structure operated in TE_{01} mode with matching circuit calculated from transmission line theory. The refractive index of the matching layer n_x is:

$$n_x = 3.079\{$$

With thickness of l_x

$$l_x = 0.92 + \frac{m \cdot \pi}{\beta_0}$$

$$\beta_0 = 2 \cdot \pi \cdot \frac{n_x}{\lambda} \quad (3.23)$$

While $m=0, 1, 2, 3, \dots$

Fig. 3.10 shows the simulated far field radiation pattern and E field co-polar (X-Y plane) plots of the two shells lens without (a1 & a2) and with (b1 & b2) impedance matching layer. X is the direction of propagation; Y is the polarization of the E field.

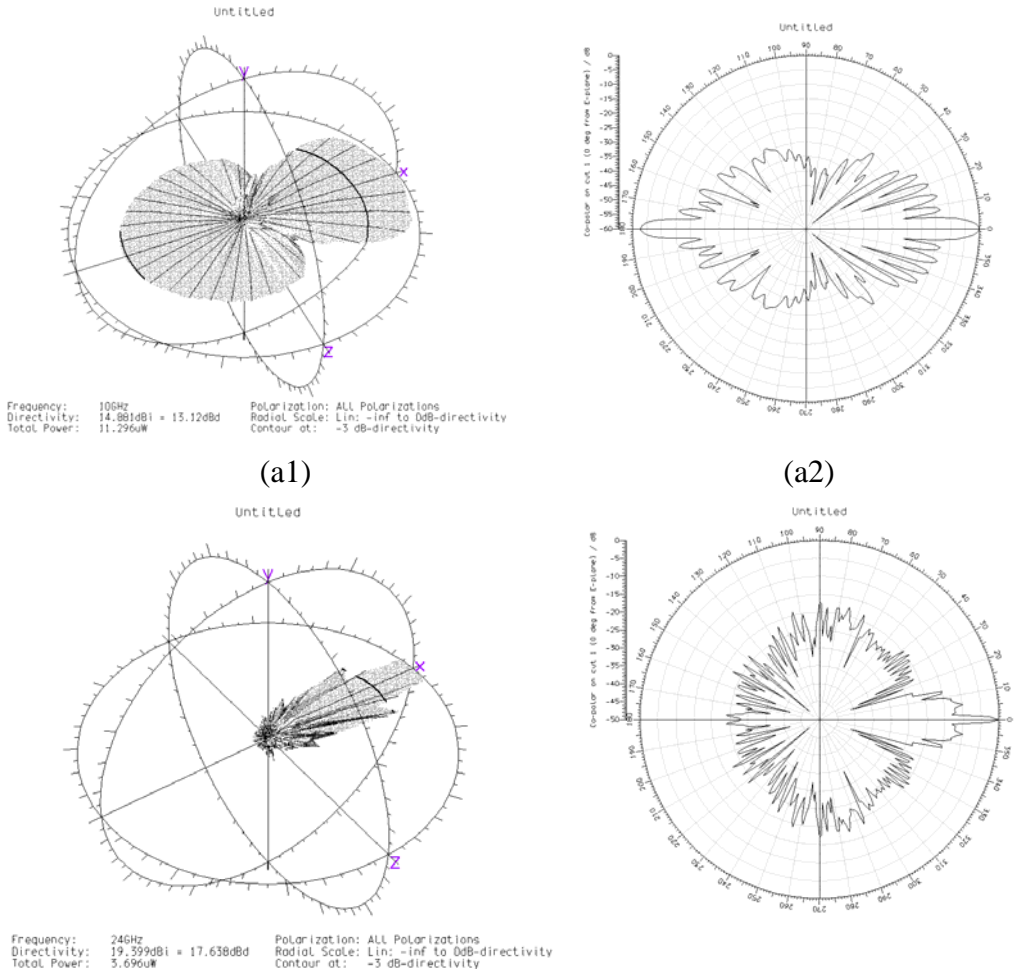


Figure 3.10 Simulated Two Shell Lens

It is apparent from Fig. 3.10 that the lens suffers large reflection due to the refractive index discontinuity. However with the impedance matching layer in position the problem is resolved.

(3.2.3) Rozendaal Lens

The microwave Luneburg lens manufactured by Rozendaal Associates, Inc. has also been investigated, [21~22]. We see from Fig. 3.11, that this three-layer stepped-index lens reflector has an effective radius between the 2.646" and 3.046". After accounting for the effect from the virtual fourth air layer, the focal point for this lens lies between the lens physical periphery and the reflector.

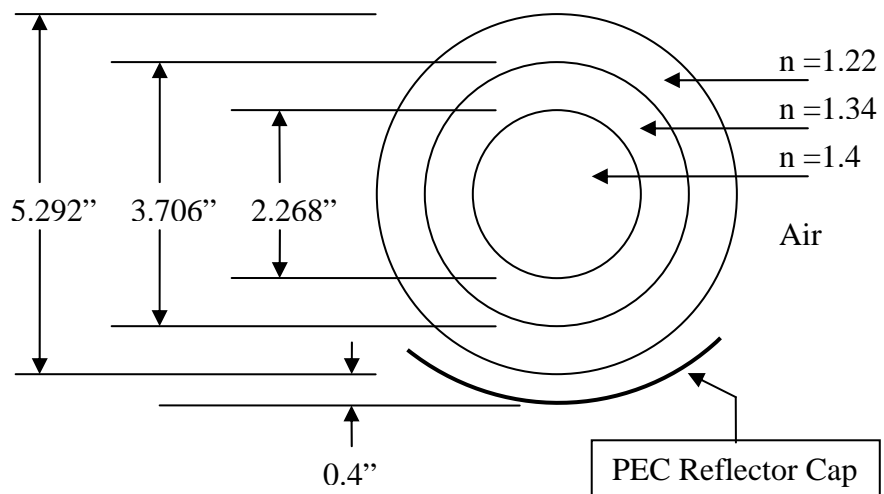


Figure 3.11 lens reflector

In fact, this lens was designed by quantizing the continuous dielectric in the conventional Luneburg lens into only three discrete values. This design could facilitate fabrication by using fewer dielectric material layers. Fig. 3.12 (a) is the simulated co-polar E field plot and (b) the field distribution of this lens reflector operated in TE_{01} mode at 24 GHz plane wave excitation (propagate from left to the right). From simulation, this lens has θ_{3dB} of 5° , comparing with the 4.5° of the ideal Luneburg lens.

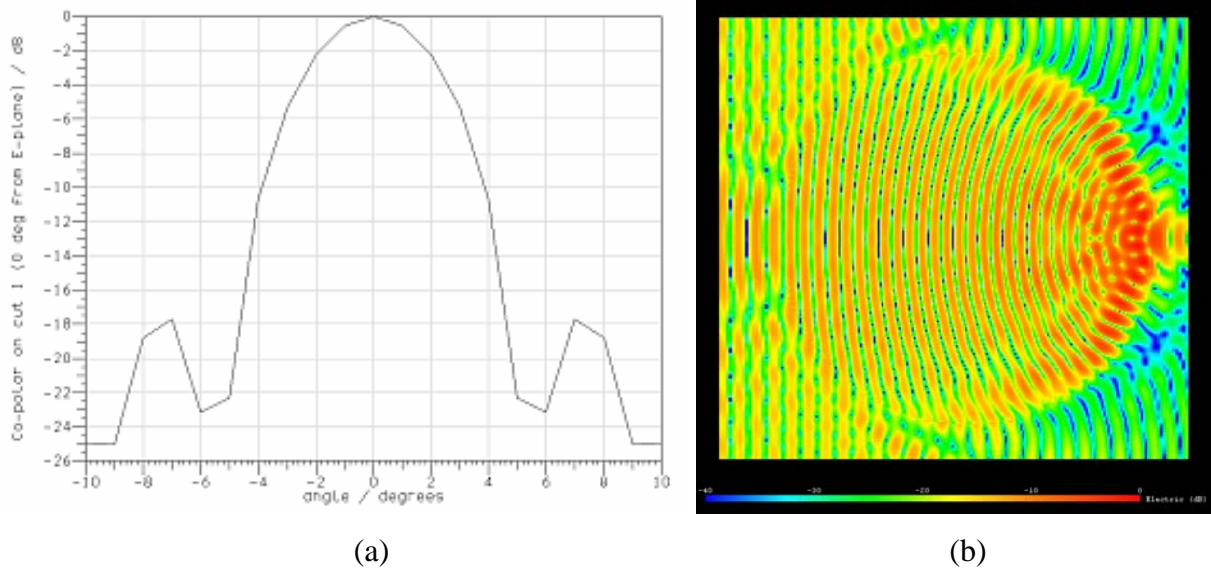


Figure 3.12 Simulated Rozendaal lens reflector at 24 GHz

(3.3) Conical-Wave Focusing Lens Synthesis

Here, the characteristics of the conical-wave focusing lenses are synthesized with the aim of establishing the design parameters required for a tuneable lens suitable for electronic scanning.

(3.3.1) 2-D Parallel-Plate Lens with TE Mode Propagation

In a parallel-plate medium with TE_{01} mode propagation (E field parallel with the plates), the effective index of refraction n is

$$n = \sqrt{\epsilon_r - \left(\frac{\lambda}{2 \cdot a}\right)^2} \quad (3.17)$$

There are four variables in (3.17). As the first step n is determined by the ray tracing theory for different focusing angles (from Fig. 3.5). When $p = 0$, the lens is a standard Luneburg Lens, then the variables in (3.17) could be modified in order to get the required n . Table 3.1 below shows the various design routes that could be adopted.

	Constant		Variable
1	ϵ	f	a
2	a	f	ϵ
3		a	ϵ f

Table 3.1

(1) Constant Frequency and Permittivity, Variable Plate Spacing

This is with the method of the conventional stepped height lens we have already built, [23]. See from Fig. 3.13, the colour represents different inclination angles of the incident plane waves. The legend values are the degrees of this angle β in the Fig. 3.4. The original Luneburg lens is when $\beta = 0$ (yellow curve in the figure below).

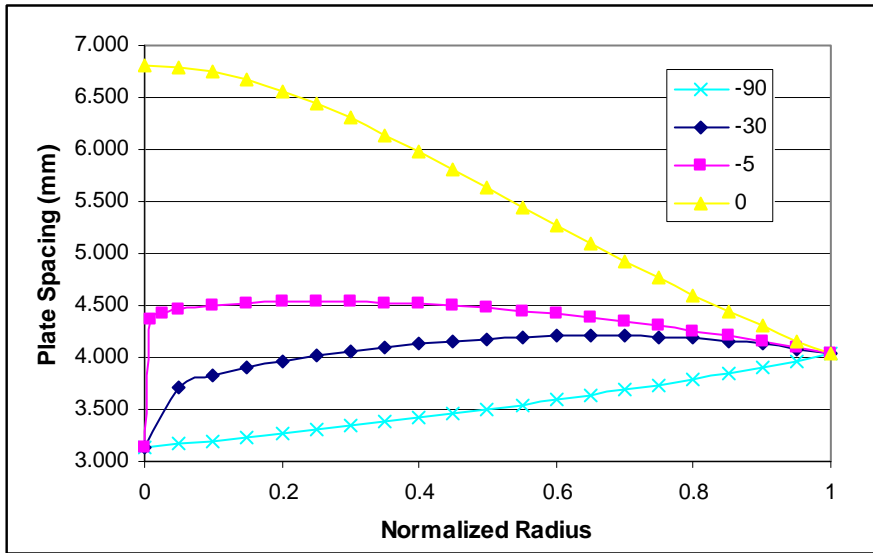


Figure 3.13 Variable plate spacing

It is noticed from Fig. 3.13 that the spacing step in this lens is very small. However, it is not convenient to get the rapid-scanning beam by changing the plate spacing mechanically. Thus other methods will be introduced.

(2) Constant Frequency and Plate Spacing, Variable Permittivity

With the lens dielectric parameters controllable by D.C bias applied to an electronically controllable permittivity e.g. nematic state Liquid Crystal, the lens could be made tuneable to produce multiple scanned conical beams. In this section, the lens structure is constant parallel plate spacing with tuneable permittivity dielectric material filled, operated in constant frequency.

$$a = \frac{\lambda}{2\sqrt{\epsilon_r - 1}} \quad (3.18)$$

$$\epsilon(r) = n^2 + \left(\frac{\lambda}{2a} \right)^2 = n^2 + \epsilon_r - 1 \quad (3.19)$$

In (3.18), ϵ_r is the initial permittivity value required to give a constant equivalent refractive index 1 at the rim of the lens, and $\epsilon(r)$ is the variable permittivity as the function of r .

When the $f = 30$ GHz, $\epsilon_r = 2.54$, the flat plate spacing a is 4.029 mm (3.18). Fig. 3.14 shows the required permittivity of each radial region for each β .

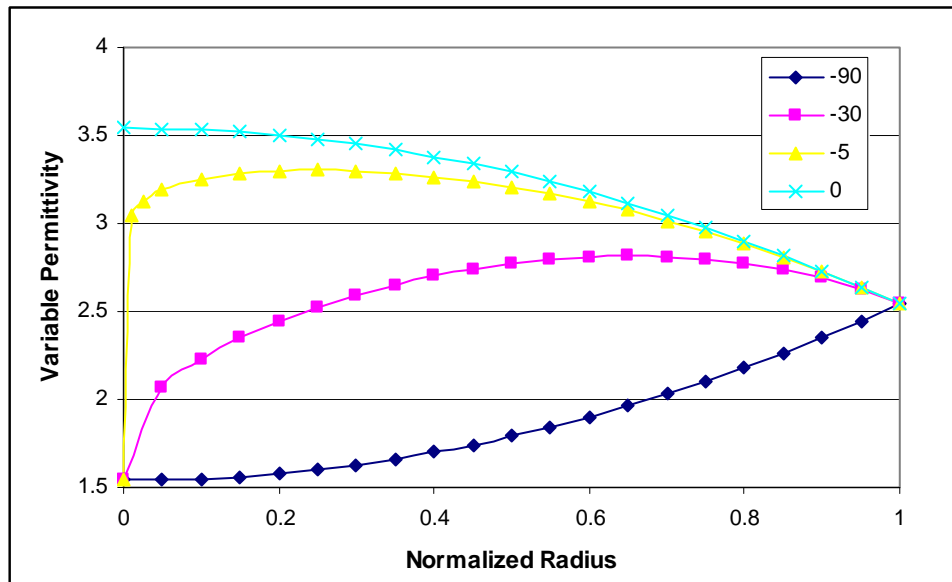


Figure 3.14 Variable permittivity

It is noted from Fig. 3.14, the Liquid Crystal (LC) permittivity variation (2~3) is suitable for the design of scanning out to -30 degrees. However, the thickness a here is too large to be available for LC applications, which should be of the order of several hundred microns, [24].

Fig. 3.15 shows a proposed structure of a partially filled thin LC layer (200 um) in the presence of a relatively thicker substrate base (several mm) composed of solid dielectric material. At the rim of the lens, the refractive index is always 1, so no LC is needed in this region.

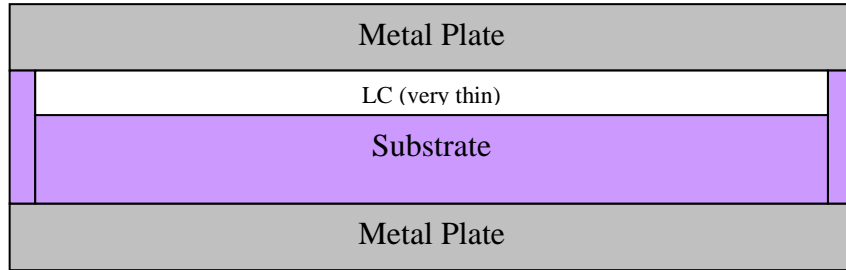


Figure 3.15 Tuneable Luneburg Arrangement

(3) Constant Plate Spacing, Variable Frequency and Permittivity

Another possibility is to hold the focal point constant as frequency is varied by modifying the radial permittivity of the material.

With a flat plate structure, if the frequency is changed from $f1$ to $f2$, the permittivity in certain radial position should also be modified to keep the $n(r)$ remain the same, so as to sustain the same focusing position of the conical beam. From (3.17),

$$\varepsilon_1 - \left(\frac{\lambda_1}{2 \cdot a} \right)^2 = \varepsilon_2 - \left(\frac{\lambda_2}{2 \cdot a} \right)^2 \quad (3.20)$$

For example, the original equivalent permittivity at the rim of the lens is $\varepsilon_2 = 2.54$ and the original wavelength is $\lambda_2 = 10$ mm (operation frequency is $f = 30$ GHz). The plate spacing is $a = 4.029$ mm to give a constant equivalent refractive index 1 at the rim of the lens, then when the wavelength changes from λ_2 to λ_1 (frequency changes), the equivalent permittivity at this position should be modified to ε_1 to maintain the original radiated beam direction.

$$\varepsilon_1 = \frac{\lambda_1^2 - 10^2}{(2 \cdot a)^2} + 2.54 \quad (3.21)$$

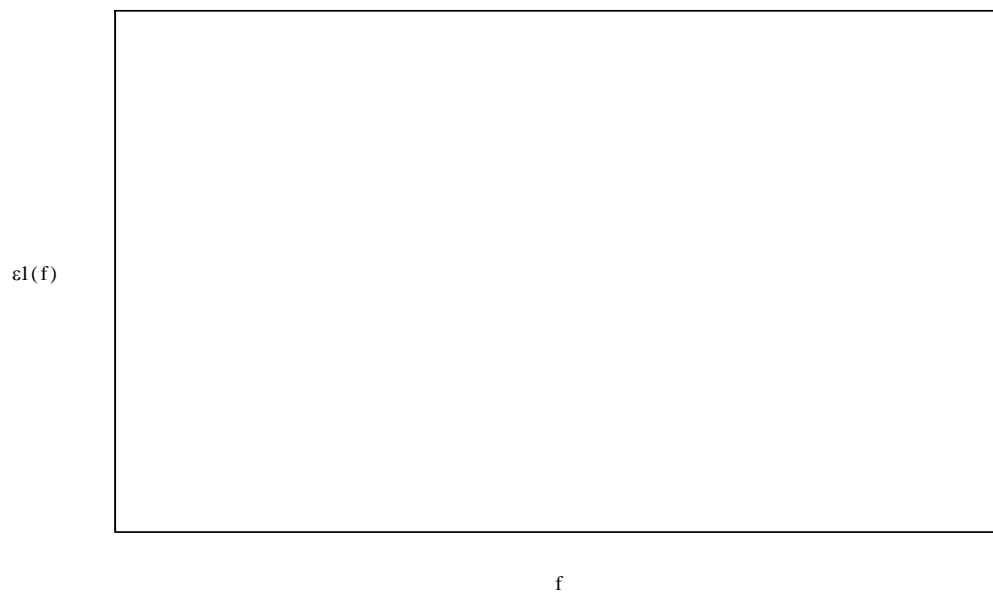


Figure 3.16 Frequency(GHz) vs. Equivalent Permittivity at norm radius 1

Fig. 3.16 shows the variation of the required permittivity variation as the frequency changes from 26 GHz to 38 GHz.

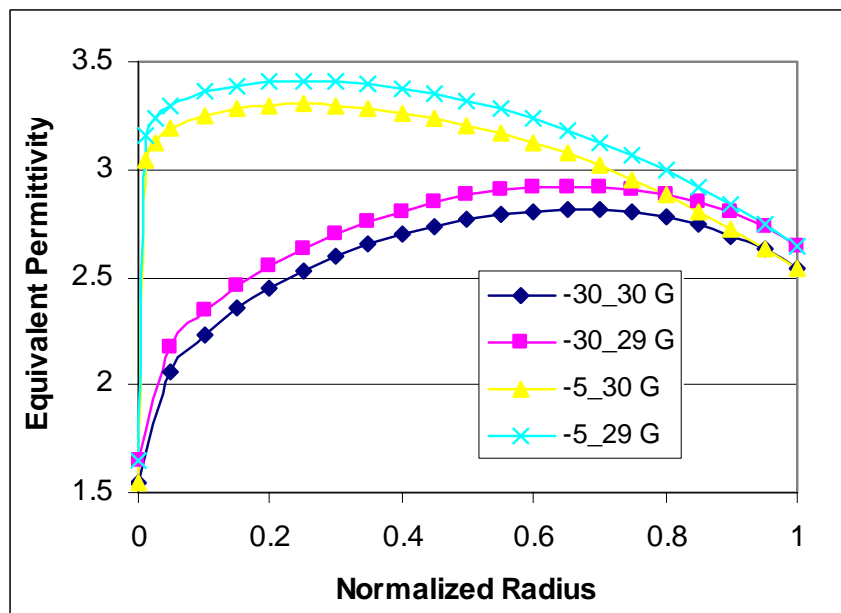


Figure 3.17 Variable frequency & permittivity

Fig. 3.17 shows the radial permittivity variation inside the lenses when the frequency alters from 30 GHz to 29 GHz while the direction of the conical radiation beam remains the same ($\beta = -5^\circ$ and $\beta = -30^\circ$).

(3.3.2) 2-D Parallel-Plate Lens with TEM Mode Propagation

In a parallel-plate medium, when the plate spacing is sufficiently small (smaller than $\lambda/2\sqrt{\epsilon_r}$), only the TEM mode can propagate (E field perpendicular to the plates). When the plates are fully filled with the dielectric material with permittivity of ϵ , the effective index of refraction n is

$$n = \sqrt{\epsilon_r} \quad (3.22)$$

It is demonstrated from the Far-Field pattern simulation that with this model and theoretical calculations of expected bandwidth in this lens, the tolerance on the plate spacing and operating frequency would be less severe with the TEM flat-plate Luneburg lens than for the TE₀₁ lens.

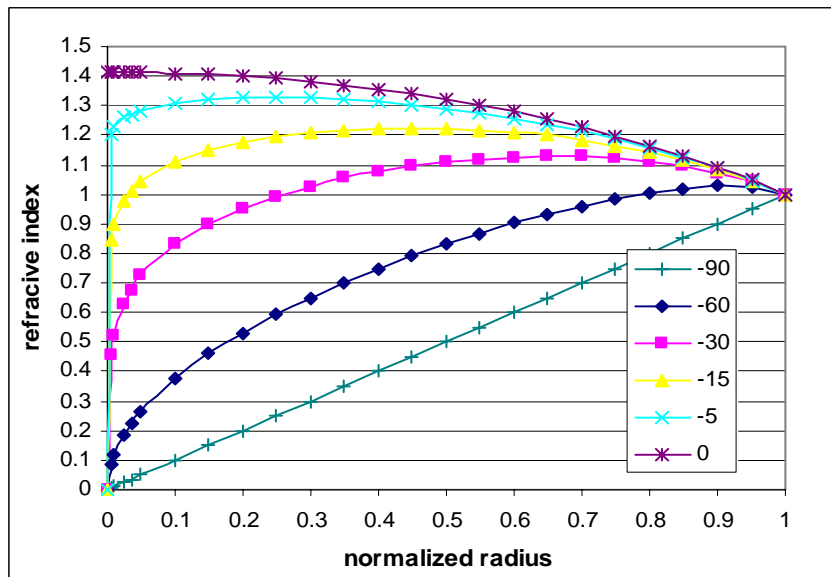


Figure 3.18

Fig. 3.18 shows the required refractive index as the function of normalized radius and directions of the radiation. This figure is equivalent to the Fig. 3.5.

Summary Conclusion Chapter 3:

The general properties of the Luneburg-Type Lens are analyzed and a class of lenses which allows the incident EM wave to focus at any required position is presented. The properties of conical wave focusing lenses are parametrically studied in order to investigate the possibility of electronic scanning the lens. Also, the possibility of quantizing the lens permittivity graduation into fewer values is also investigated so as to facilitate design and fabrication. It is shown that an additional impedance matching layer is needed in order to rematch the lens to free space.

IV. Liquid Crystal Material Properties

Conventional nematic liquid crystal (LC) has large insertion loss when used in resonant structures. This limits use to non-resonant structures such as phase shifters or non-resonant antennas e.g. a microwave lens. As the LC material is always very lossy, the typical loss tangent is above $\tan \delta = 0.02$, it is best to operate with thick liquid crystal layers (up to 500 μm) and off resonance so that losses are low, [24]. Literature, [25~28], shows that around 60 to 70 degrees of phase shift per dB of loss can be achieved, for bias voltages from 10 to 100 V dc which is very low comparing with other tuneable material (ferrite e.g.) applications. Also, the typical permittivity value of LC K15 is from 2 to 3.5, so it is appropriate to be used in the Luneburg Lens design, [29].

(4.1) Test Arrangement of Tuneable Patch Element (In progress)

The 10 GHz waveguide simulator filled with LC controlled tuneable patch elements has been manufactured. Fig. 4.1 shows the structure of the test arrangement.

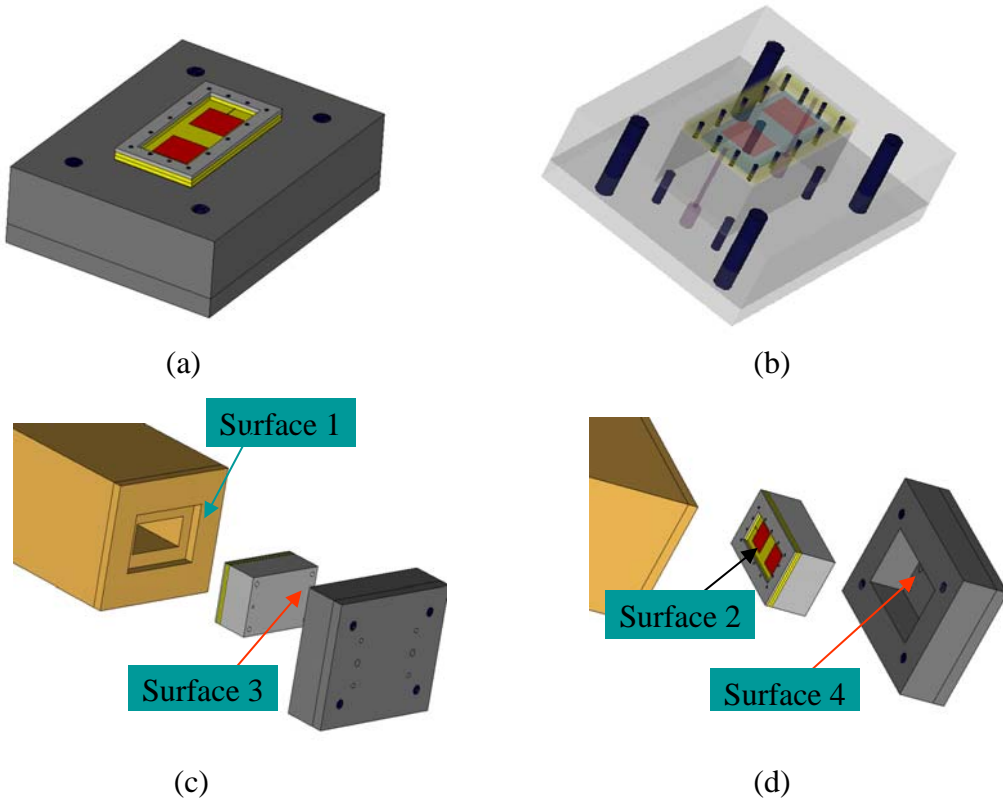


Figure 4.1 Test waveguide arrangements

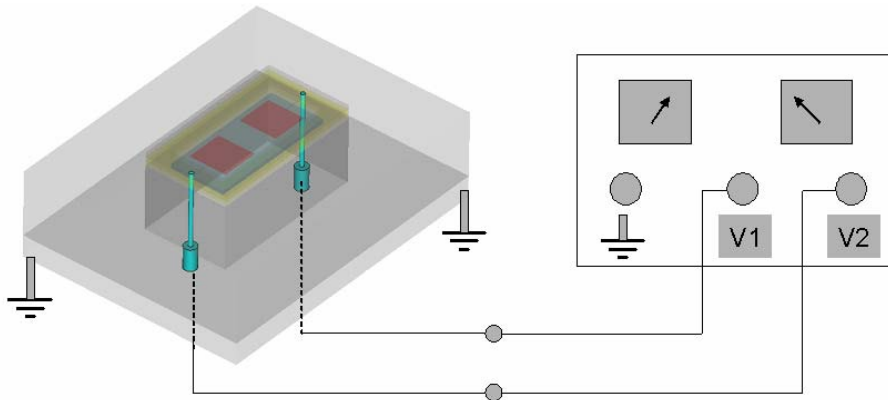


Figure 4.2

Fig. 4.2 shows the DC controlled tuneable patch including the wire connection used to introduce DC voltage control. Patch 1 and 2 can be controlled individually by V1 and V2 so as to modify the equivalent permittivity.

(4.2) Collaboration required to Progress Material (in progress)

In order to create the required liquid crystal material to the engineering specification needed for practical demonstrations for this and another related project on tunable frequency selective surfaces we have identified various industrial collaborators, namely:

1. Liquid crystal material:

Merck, Germany [30] and R & D Merck, UK [31] --- contacted;

2. Main frame of the Multilayer Dielectric Liquid Crystal (MDLC):

Liquid Crystal Polymer (LCP) Rogers Corporation [32] --- contacted;

4. LC molecule alignment, the most advanced topic on device assembly:

Polyimide: SE-150 from Nissan [33] --- contacted; (seeking for better supplier)

Rubbing machine, help from Exeter University [34] --- design started;

5. Ultra smooth surface on LCP substrate:

Hot lamination --- technical support from R & D Rogers [32];

Surface polishing --- free sample from QED Technologies [35];

6. Adhesive material:

Master bond [36] and Norland [37] --- contacted;

(4.3) Concept for Tuneable Lens Fabrication

The tuneable lens configuration should permit the inclusion of d.c. controllable dielectric material (LC) into a Luneburg Lens in order to modify the radial permittivity so as to make the lens capable for electronic scanning.

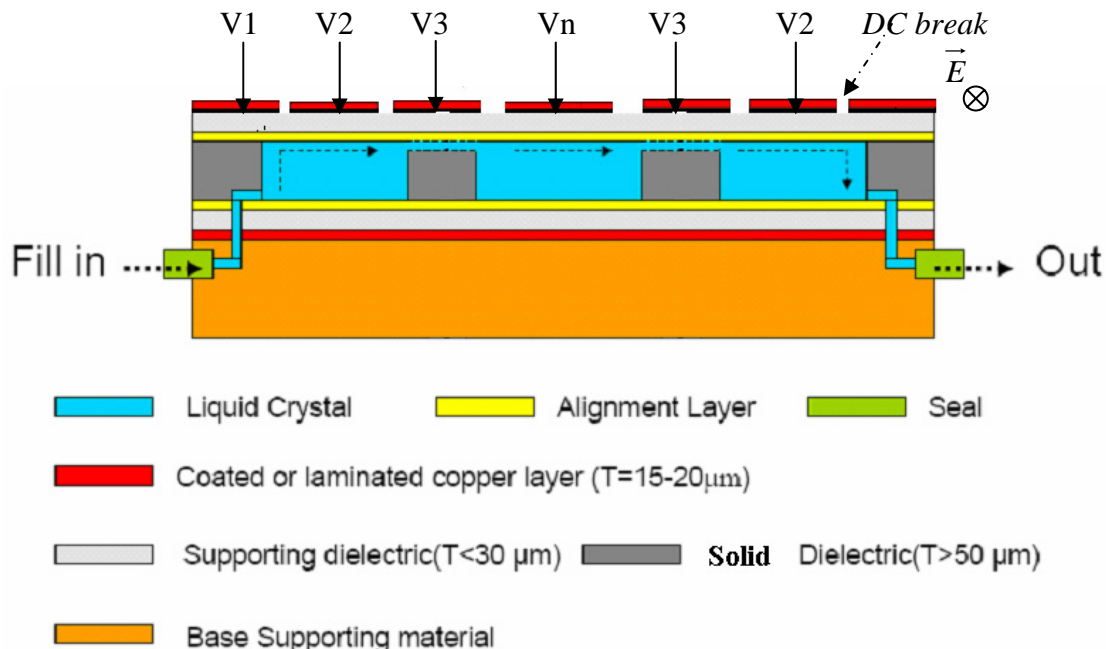


Figure 4.3 Proposed MDLC tuneable lens configuration

Fig. 4.3 shows the proposed tuneable lens configuration operated in TE_{01} mode, where the E field polarization is parallel with the metal plate. The lens is quantized into several electrically dc isolated regions, each of which is connected with an individual d.c. supply to have its localised radial permittivity controlled. Annular d.c. breaks are introduced on the top metal plate in order to isolate the biasing voltages from each other. As the E field polarization is orthogonal to these dc breaks, little energy leakage would occur. Further work will need to focus on the investigation of the coupling between these d.c. breaks.

V. Reflection Amplifier

The possibility of arranging the one port reflection amplifiers (RA) along the periphery of the planar Luneburg lens to form active lens reflector is considered. The inclusion of the RA could enhance the reflection properties of the lens.

The design of the reflection amplifier is similar to that of an oscillator. The reflection coefficient Γ (S11) at the input port of the circuit is:

$$\Gamma = \frac{Z_{in} - Z_s}{Z_{in} + Z_s} \quad (5.1)$$

where Z_{in} is the input impedance of the one port circuit to be designed and Z_s is the output impedance (usually 50Ω at the designed frequency). For oscillator mode, the real part of $Z_{in} + Z_s$ is negative and the imaginary part is set to be zero at the desired frequency. For reflection amplifier mode, the real part should be designed to have a small absolute value to obtain a high reflection gain and the imaginary part is nonzero to avoid self oscillation. Both circuits need negative input resistance.

The reflection amplifier (RA) in this investigation is designed using the device OMMIC D01PHNI1, a PHEMT FET (Pseudomorphic High Electron Mobility Transistor), [3] and GaAs substrate under MMIC process with the total size of 1.5 mm by 2 mm. From the preliminary ADS simulation [38], this RA could produce 14 dB Gain when operated at 24 GHz.

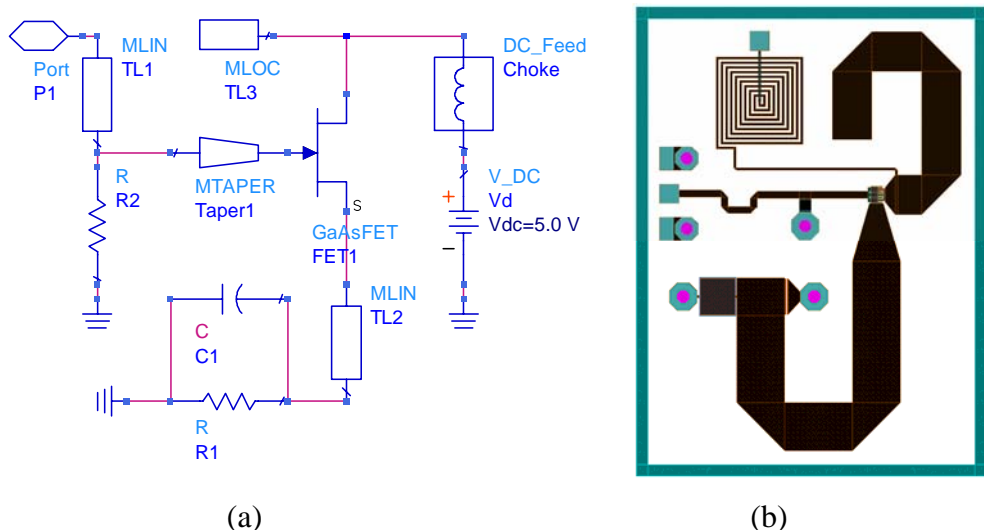


Figure 5.1 Schematic of the Reflection Amplifier

Fig. 5.1 shows (a) the circuit diagram of the reflection amplifier; (b) the layer schematic of this chip. A dc voltage ($V_{dc} = 5$ V) is applied to the drain of the device through a high impedance choke. The source is connected to ground through a resistor ($R1$) in parallel with an ac bias capacitor ($C1$). This source resistor would result in a negative-bias voltage between the gate and source terminals, and also introduce a negative feedback path stabilize the biasing current. In order to produce a negative input resistance, i.e. the device operate in the unstable region, a section of microstrip line ($TL2$), which is equivalent to a series inductor, is inserted between the device's source terminal and source resistor. Also, an open-ended microstrip line ($TL3$) is connected to the drain terminal. Both $TL2$ and $TL3$ are tuned to yield the negative input resistance at the required frequency (24 GHz). A transformer is used to transform the negative input impedance at the gate to a value near -50Ω . Also, a shunt resistance ($R2$) is added at the input 50Ω line ($TL1$).

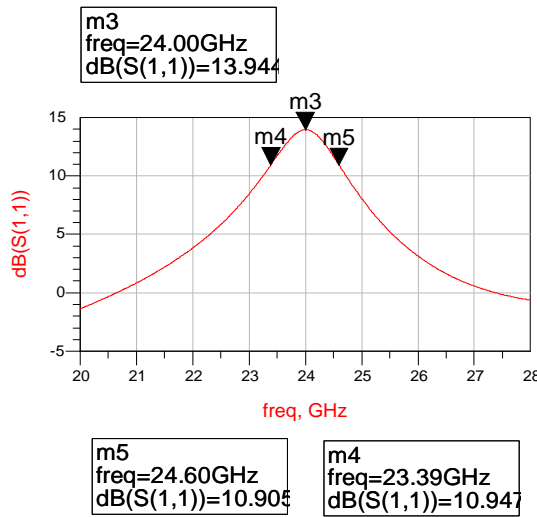


Figure 5.2 Simulated S₁₁ of the circuit

Figure 5.2 shows the simulated Gain (S₁₁) of this one port circuit is 13.94 dB at 24 GHz, with the input impedance of $Z_{in} = -50.44 + j20.6 \Omega$. Use this Z_{in} in (5.1), the reflection coefficient $\Gamma = 13.943$ which is agree with the simulated S₁₁. The frequency range of -3 dB Gain is from 23.4 GHz to 24.6 GHz.

Further work will be focused on the optimization of the circuit design to increase the gain within the refection amplifier operation mode.

VI. Conclusions and Future Work

Various Luneburg Lens structures have been designed. Suitable artificial dielectrics are demonstrated to be capable of being built by drilling holes into dielectric sheet or by etching holes into one or both faces of the metallization on a PCB. It was shown that by the extension of the lens with an additional impedance matching layer the internal construction of the lens could be quantized into fewer values so as to facilitate fabrication. The general properties of the Luneburg-Type Lens were presented and a class of lenses which could transform an incident plane EM wave to a focus at any required position were derived based on the ray tracing geometry. Some variants of these lenses were synthesized in order to demonstrate the feasibility of the eventual formation of a tuneable lens capable of electronically conical scanning or focal length control by using the Liquid Crystal material as a tuneable substrate in future work. Also attention was given to the design of a planar lens fabricated on standard PCB, by using a holey metal plate method. This structure could eventually lead to an ultra thin lens. Finally it was shown that by adding reflection amplifiers along the periphery of the lens it should be possible to enhance its reflection capability.

VII. Appendix

(A) Holey Metal Plate Luneburg Lens : TE mode

Operating at 24 GHz; the radius of the lens are 152.4mm;

Unit : mm			Holes Rectangular Lattice		
region	ϵ_{eq}	physical radius	Δ of physical radii	b	d
1	2	0.00	34.08	2.00	1.40
	1.95	34.08			
2	1.9	48.19	24.95	1.85	1.30
	1.85	59.02			
3	1.8	68.16	17.18	1.95	1.30
	1.75	76.20			
4	1.7	83.47	13.96	1.83	1.20
	1.65	90.16			
5	1.6	96.39	12.07	1.96	1.20
	1.55	102.23			
6	1.5	107.76	10.79	1.87	1.10
	1.45	113.02			
7	1.4	118.05	9.85	2.07	1.10
	1.35	122.87			
8	1.3	127.51	9.11	2.05	1.00
	1.25	131.98			
9	1.2	136.31	8.52	2.12	0.90
	1.15	140.51			
10	1.1	144.58	8.04	2.05	0.70
	1.05	148.54			
air	1	152.40			

Table A

b: the central spacing of the adjacent holes;

d: the diameter of the holes;

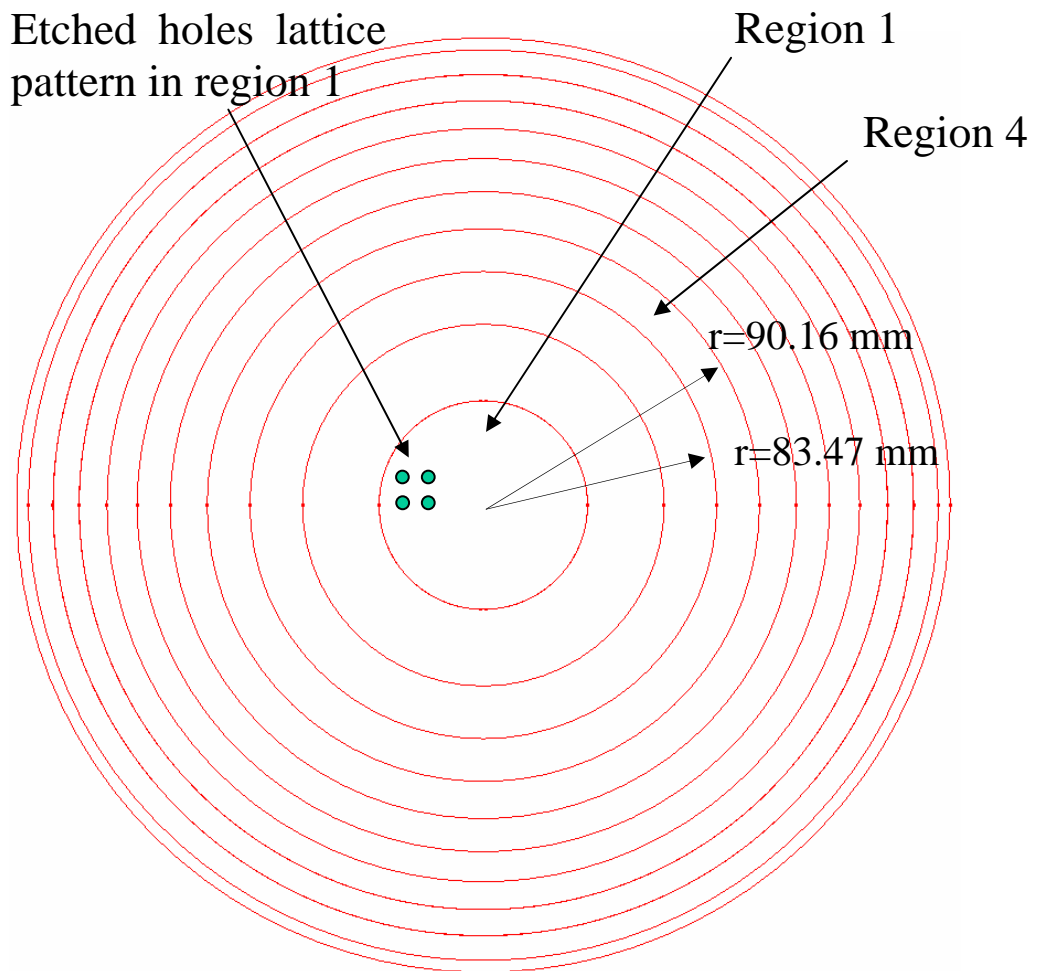


Figure A

See from Fig. A, in region 4, the radii are from 76.2 mm to 90.16 mm, (Δ of physical radii is $90.16 \text{ mm} - 76.2 \text{ mm} = 13.96 \text{ mm}$). In order to get the equivalent permittivity ($\epsilon = 1.7$) in this region, the holes are etched on the top metal plate with rectangular lattice, the central spacing of the adjacent holes $b = 1.83 \text{ mm}$ and the diameter of the holes is $d = 1.2 \text{ mm}$.

(B) Holey Metal Plate Luneburg Lens : TEM mode

$f = 24 \text{ GHz}$, $\lambda_0 = 12.5 \text{ mm}$;

a is the spacing between the plates; $a < \lambda / (2\sqrt{\epsilon_r})$; air filled, $\epsilon_r = 1$; $a = 0.5 \text{ mm}$;

d is the diameter of the holes; $d = 0.2, 0.4 \dots 1 \text{ mm}$;

b is the distance between the neighbouring holes; $b = 1, 2 \text{ mm}$;

l is the longitude length of the simulated parallel plate; $l = 10 \text{ mm}$;

Table B shows the variation of wavelength under this structure. The simulation value has an error of about 2 degrees with respect to the theoretical value. In the Table, the structure “ $d**b**$ ” represents the holes on the metal plate having diameters of d and nearest neighbour spacing of b . It is apparent that, except the case “ $d0.5 b1$ ”, in all the other cases the leaky energy is same according to the observed S-parameter values. When the ratio of hole removal increases to 50.3% (“ $d0.8 b1$ ” case), the phase shift changes most, which is from 69.85° to 56.75° , i.e. the equivalent guide wavelength varies from 12.5 mm (no holes) to 11.8 mm.

structure	Δ (ratio of removal)	Phase S21	Mag S21	Mag S11
no holes	0	69.85	> 0.9	<0.02
d0.2 b2	0.79%	69.63		
d0.4 b2	3.10%	68.91		
d0.6 b2	7.10%	68.59		
d0.8 b2	12.60%	66.7		
d1 b2	19.60%	62.42		
d0.8 b1	50.30%	56.75		
d1 b1	78.50%	26		

Table B

References

- (1) R. K. Luneburg, The Mathematical Theory of Optics, Brown University Press, Providence, Rhode Island, 1944, 208-213.
- (2) Office of Communications, Radio Location,
<http://www.ofcom.org.uk/radiocomms/isu/ukfat/?a=87101>.
- (3) <http://www.ommic.com/>
- (4) K., Sato and H., Ujie, A Plate Luneberg Lens with the permittivity Distribution Controlled by Hole Density, Electronics and Communications in Japan, Part 1, Vol. 85, No. 9, 2002.
- (5) H., Jasik, Antenna Engineering Handbook, Chap. 15, McGraw-Hill Book CO, INC., 1961.
- (6) N. Grigoropoulos and P. R. Young, Low Cost Non Radiative Perforated Dielectric Waveguide, EuMW 8, 2003.
- (7) R. C. Hansen, Microwave Scanning Antennas, Vol. 1, Academic Press, 1964, pp. 232-233.
- (8) Eccostock®0005, Emerson & Cuming Microwave Products.
- (9) G. D. M. Peeler and D. H. Archer, A Two-Dimensional Microwave Luneberg Lens, IRE Trans. Antennas Propagation, vol. 1, pp. 12 - 23, July 1953.
- (10) Micro-Stripes V6.5, Flomerics Limited, 2005.
- (11) Automotive short-range radar equipment at 24 GHz (spectrum band 21.65 to 26.65 GHz), <http://www.ofcom.org.uk/consult/condocs/24ghz/>.
- (12) LPKF, Protomat C60, <http://www.lpkf.com/index.htm>;
- (13) C. H. Walter, "Surface-Wave Luneberg Lens antennas," IRE Transactions on Antennas and Propagation, 1960;
- (14) J. Brown, "Artificial Dielectrics having Refractive Indices Less Than Unity," Proc. Inst. Elect. Engrs 100, Institution Monograph, May 1953;
- (15) Arthur A. Oliner, "The Impedance Properties of Narrow Radiating Slots in the Broad Face of Rectangular Waveguide, Part I Theory," IRE Transactions on Antennas Propagation, 1956;
- (16) L. O. Goldstone and A. A. Oliner, "Leaky-Wave Antennas I: Rectangular Waveguides," IRE Trans. Antennas Propagation, 1959;

- (17) Taconic Cer10, <http://www.taconic-add.com/en--index.php>;
- (18) S. Cornbleet, "Microwave and Geometrical Optics," Academic Press, 1994;
- (19) J. Richard Huynen. "Theory and Design of a Class of Luneburg Lenses," IRE Wescon Convention Record, Aug. 1958;
- (20) Toraldo di Francia, "Spherical lenses for Infrared and Microwaves," J. Appl. Phys. 32, 1961;
- (21) Rozendal Associates, Inc. (located at 9530 Pathway Street, Santee, CA 92071 USA);
- (22) Charles S. Liang, Donald A. Streater, Jian-Ming Jin, Eric Dunn, and Timothy Rozendal, "A Quantitative Study of Luneberg-Lens Reflectors," IRE Magazine on Antennas and Propagation, Vol. 47, No. 2, 2005;
- (23) L. Xue, V. Fusco, "Two-Dimensional Stepped Height Luneburg Lens," Loughborough Antennas & Propagation Conference, pp. 10-13, 2004;
- (24) David M. Pozar, Stephen D. Targonski, and H. D. Syrigos, "Design of Millimeter Wave Microstrip Reflectarrays," IRE Transactions on Antennas and Propagation, Vol. 45, No. 2, 1997;
- (25) Martin, N., Laurent, P., Person, C., Celin, P., Hubert, F., "Patch Antennas adjustable in frequency using Liquid Crystal," pp 699-702, Proc of 33rd European Microwave Conf. Munich, Oct 2003;
- (26) Yang, F, Sambles, J.R., "Determination of the Microwave permitivities of Nematic liquid Crystals using a single-metallic Slit Technique," Applied physics Letters, Vol. 81, No.11, pp2047-2050, Sept 2002;
- (27) D. Dolfi, M. Labeyrie, P. Joffre and J. P. Huignard, "Liquid Crystal Microwave phase shifter," Vol. 29, No. 10, Electronics Letters, 1993;
- (28) Takao Kuki, Hideo Fujikake, and Toshihiro Nomoto, "Microwave Variable Delay Line Using Dual-Frequency Switching-Mode Liquid Crystal," IRE Transactions on MTT, Vol. 50, No. 11, 2002;
- (29) Rolf Jakoby, etc, "Broad-Band Microwave Characterization of Liquid Crystals Using a Temperature-Controlled Coaxial Transmission Line," IEEE Transactions on Microwave Theory and Techniques, Vol. 53, No. 6, pp 1937-1945, June 2005;
- (30) <http://www.merck.de/servlet/PB/menu/1001723/index.html>;

- (31) <http://pb.merck.de/servlet/PB/menu/1213610/>;
- (32) <http://www.rogerscorporation.com/index.htm>;
- (33) Nissan Chemical Industries Ltd. <http://www.nissanchem.co.jp/english/>;
- (34) School of Physics, University of Exeter,
http://newton.ex.ac.uk/research/emag/liq_cryst/;
- (35) QED Technologies; <http://qedmrf.com/orgMain.asp>;
- (36) <http://www.masterbond.com/>;
- (37) <https://www.norlandprod.com/adhesives/adhchart.html>;
- (38) Advanced Design System 2003C, Agilent EEsof EDA;